TOPOLOGICAL PHASES INDUCED BY KONDO COUPLING IN $R_2Ir_2O_7$

Gang Chen
CU-Boulder

Colorado Physics
Department of Physics•University of Colorado at Boulder
JILA
NIST&CU

Collaborator: Michael Hermele

OUTLINE

- Introduction
- Model Hamiltonian
- Phase diagram
- Experimental relevance

- S=1 “Quantum spin liquid”: quantum criticality in $Ba_3NiSb_2O_9$

OUTLINE

- Introduction
- Model Hamiltonian
- Phase diagram
- Experimental relevance

$R_2Ir_2O_7$: both exotic and topological?

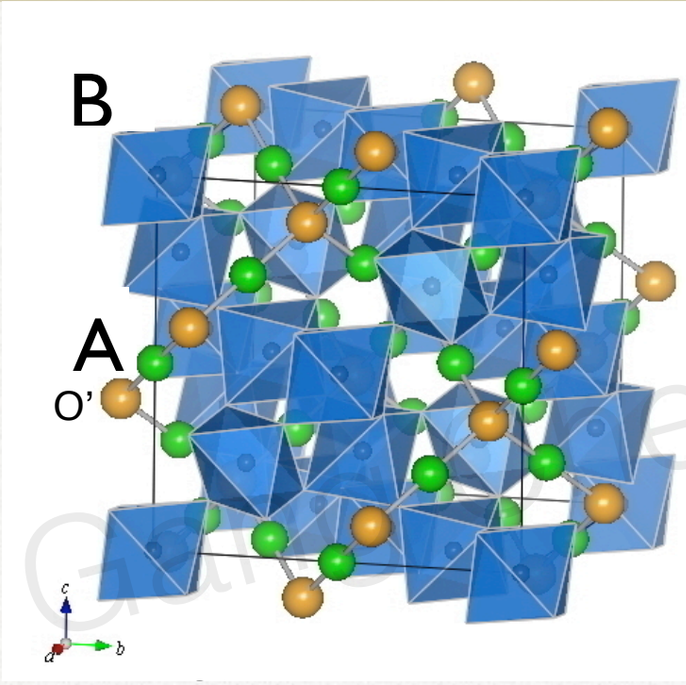

A=R
B=Ir

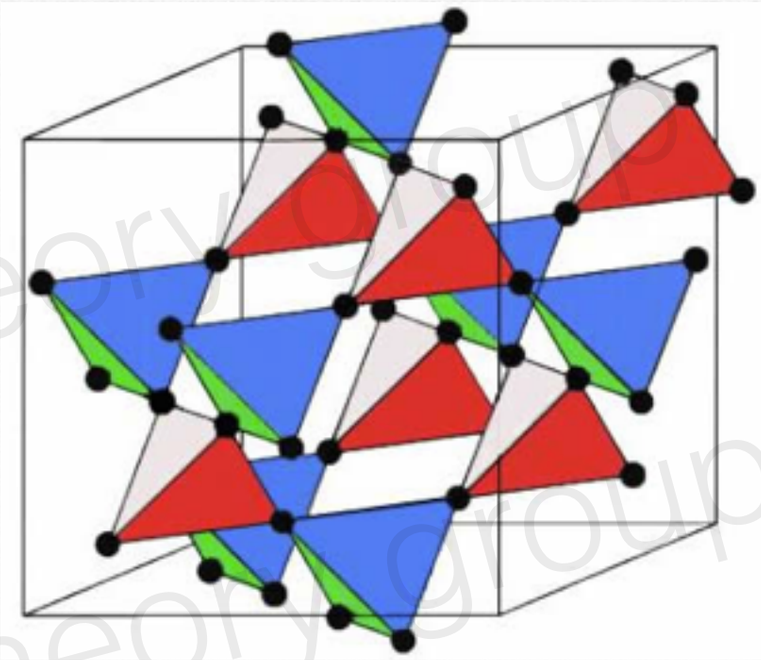

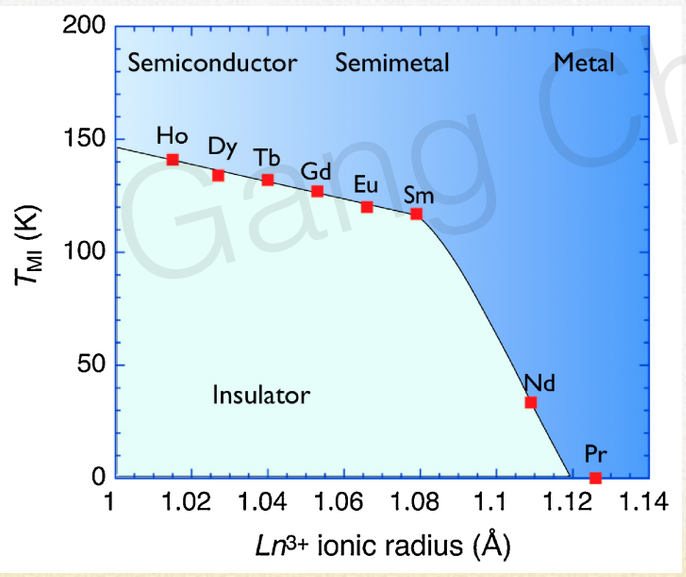

Strong SOC in Ir

$$\lambda \sim 0.5eV$$

Yanagishima et al JPSJ 2001
Matsuhira et al, JPSJ 2002
Matsuhira, et al JPSJ 2007

Classical Spin ice -> Quantum spin ice (@Friday Sungbin Lee)

EXOTIC PERSPECTIVE
TOPOLOGICAL MOTT-INSULATOR (TMI)

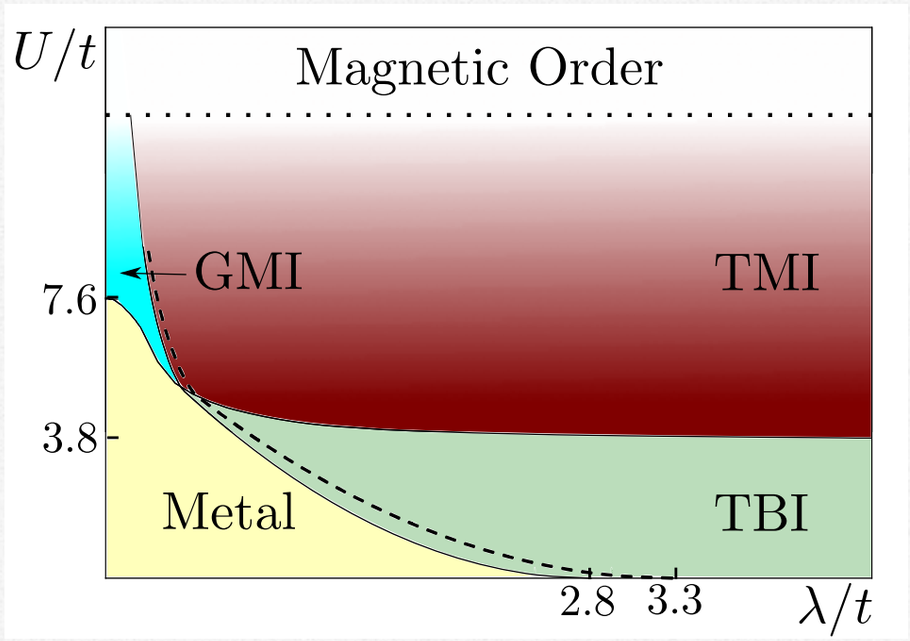

MIT driven by correlation?

Exotic phase by slave-rotor MFT: TMI

However, commensurate magnetic order in $Eu_2Ir_2O_7$!

D. Pesin, L. Balents, 2010
S. Zhao, et al arXiv 2011

ANOTHER PERSPECTIVE
WEYL SEMIMETAL (WSM)

LSDA+SOC+U

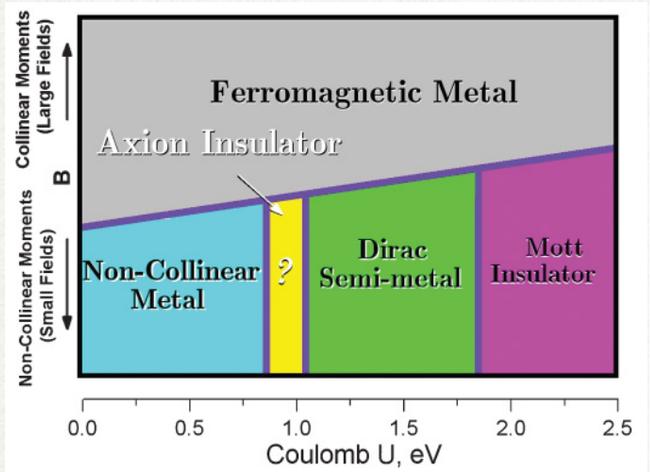

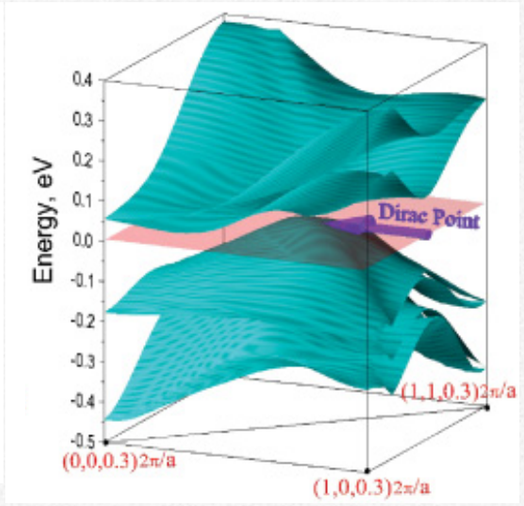

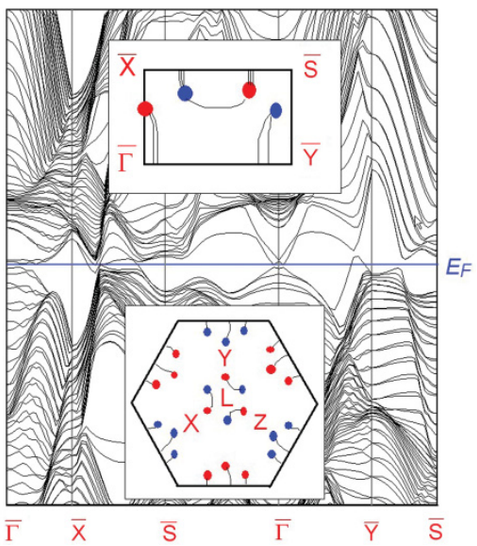

24 Weyl points predicted in $Y_2Ir_2O_7$

Tight-binding+HF MFT

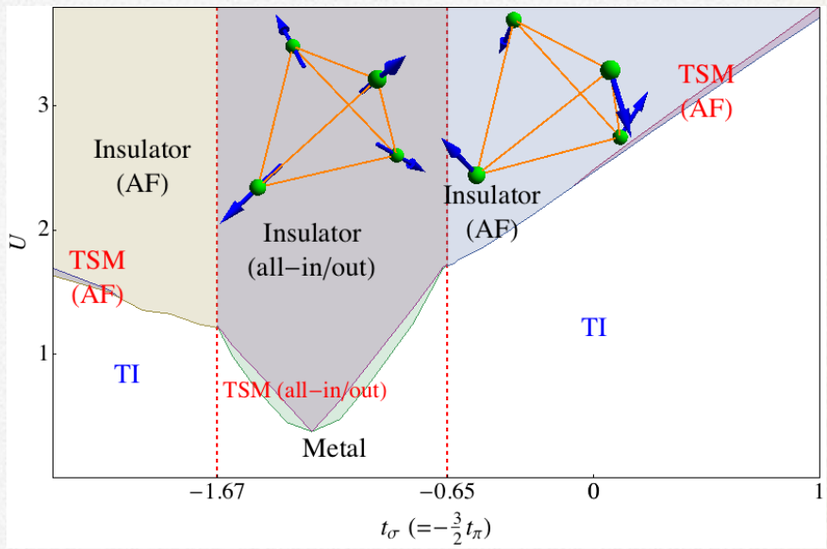

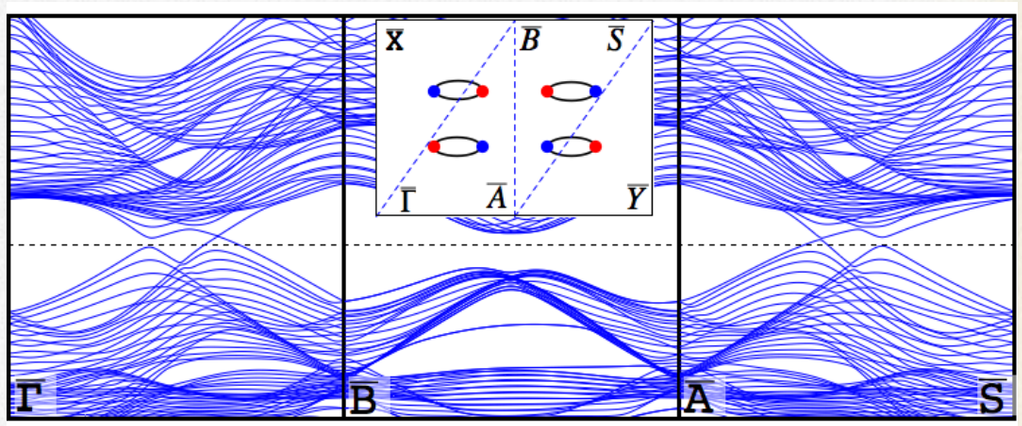

MIT driven by correlation?
WSM may be narrow.

X. Wan, et al, 2010
Witczak-Krempa et al, 2011

WSM IN TI-NI HETEROSTRUCTURE

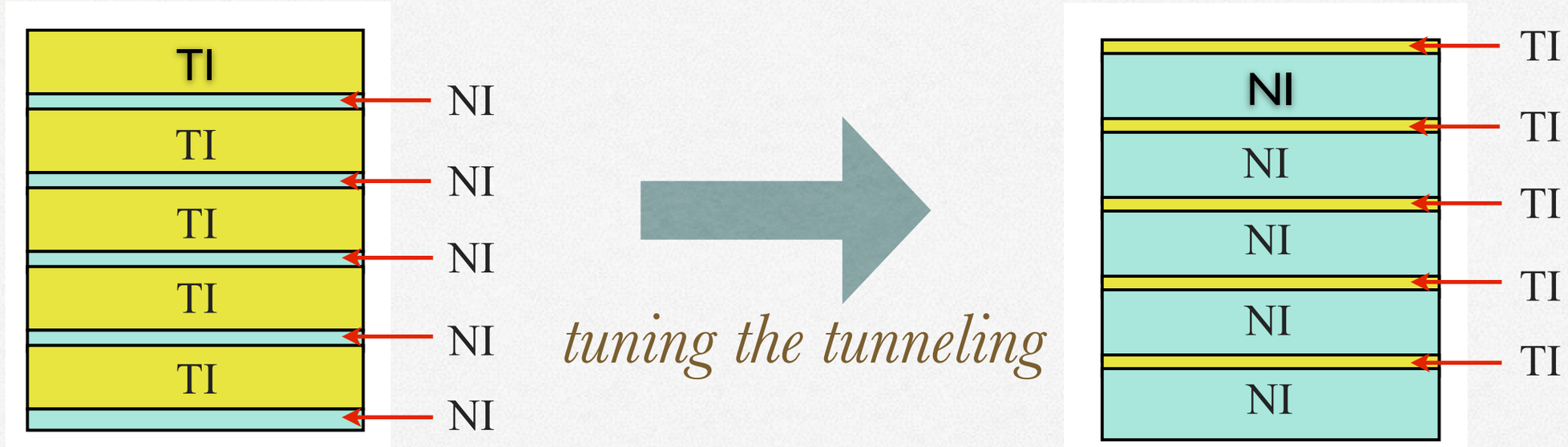

Splitting the Dirac point at QCP into 2 Weyl points by breaking T or I

Elementary WSM

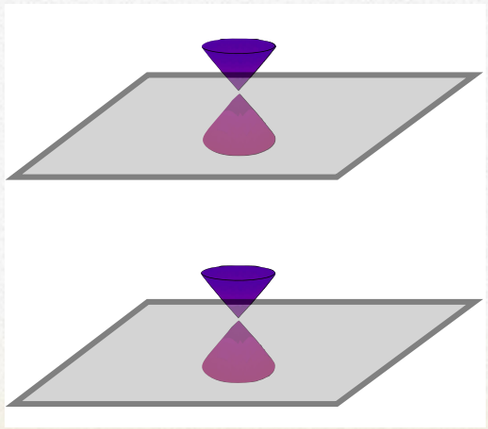

Burkov, et al 2011
Halasz, et al 2011

AXION INSULATOR

Magnetoelectric coupling

$$\alpha_{ij} = \left.\frac{\partial M_j}{\partial E_i}\right|_{\mathbf{B}=0} = \left.\frac{\partial P_i}{\partial B_j}\right|_{\mathbf{E}=0},$$

Axion response

$$S_0 = \tfrac{1}{8\pi}\int d^3x dt \left(\varepsilon \mathbf{E}^2 - \tfrac{1}{\mu}\mathbf{B}^2\right)$$

$$\Delta\mathcal{L}_{EM} = \frac{\theta e^2}{2\pi h}\mathbf{E}\cdot\mathbf{B} = \frac{\theta e^2}{16\pi h}\epsilon^{\alpha\beta\gamma\delta}F_{\alpha\beta}F_{\gamma\delta}.$$

$\theta = \pi \pmod{2\pi}$ *in STI*

Breaking T, preserving I of STI

Require: magnetism, strong SOC

d, f ↕ *4d, 5d, f* ↕

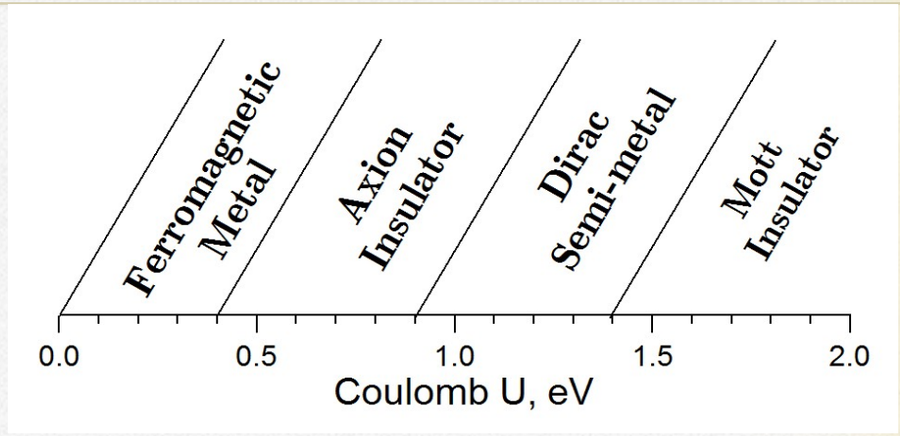

FIG. 3: Sketch of the predicted phase diagram for spinel osmates.

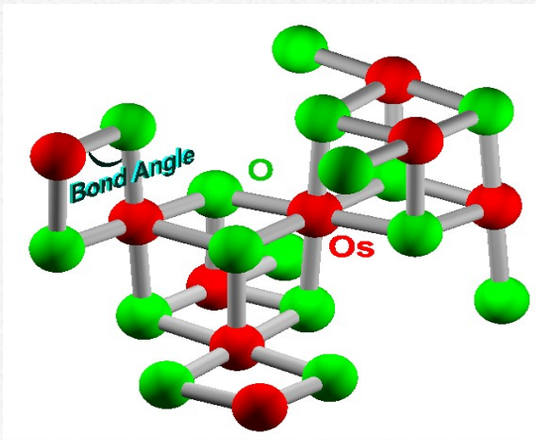

$CaOs_2O_4$
$SrOs_2O_4$
$BaOs_2O_4$
$Y_2Ir_2O_4$

Spinels: also contain pyrochlore

Qi et al 2008,
Essin et al 2009
Turner et al 2010
Wan et al 2011

OUTLINE

- Introduction
- Model Hamiltonian
- Phase diagram
- Experimental relevance

WHY KONDO?

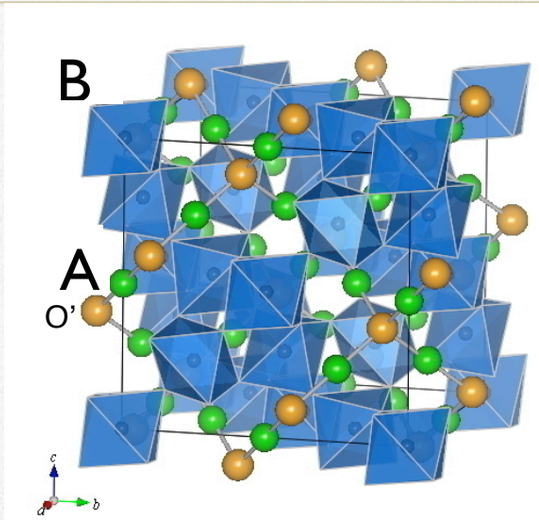

$R_2Ir_2O_7$

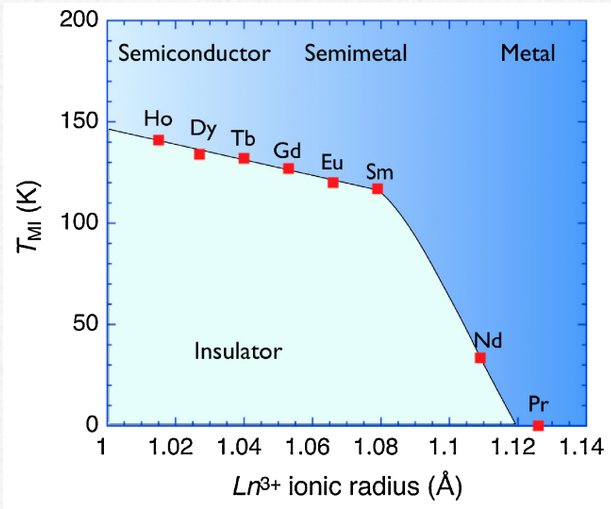

58	59	60	61	62	63	64	65	66	67	68	69	70	71
Ce	**Pr**	**Nd**	**Pm**	**Sm**	**Eu**	**Gd**	**Tb**	**Dy**	**Ho**	**Er**	**Tm**	**Yb**	**Lu**
Cerium	Praseodymium	Neodymium	Promethium	Samarium	Europium	Gadolinium	Terbium	Dysprosium	Holmium	Erbium	Thulium	Ytterbium	Lutetium
140.116	140.907 65	144.242	(145)	150.36	151.964	157.25	158.925 35	162.500	164.930 32	167.259	168.934 21	173.04	174.967

Localized f electron

Non-Kramer's ions	Kramer's ions
Pr^{3+}, Tb^{3+}, Ho^{3+}	Nd^{3+}, Sm^{3+}, Gd^{3+}, Dy^{3+}, Yb^{3+}
$4f^2, 4f^8, 4f^{10}$	$4f^3, 4f^5, 4f^7, 4f^9, 4f^{13}$

TABLE I. Non-Kramer's and Kramer's ions R^{3+} and their electron configurations.

KONDO COUPLING

$$\mathrm{Pr}^{3+} \quad J = 4$$

Non-Kramer's doublets

$$|\tau^z = \pm\frac{1}{2}\rangle = \alpha|J^z = \pm 4\rangle + \beta|J^z = \pm 1\rangle - \gamma|J^z = \mp 2\rangle$$

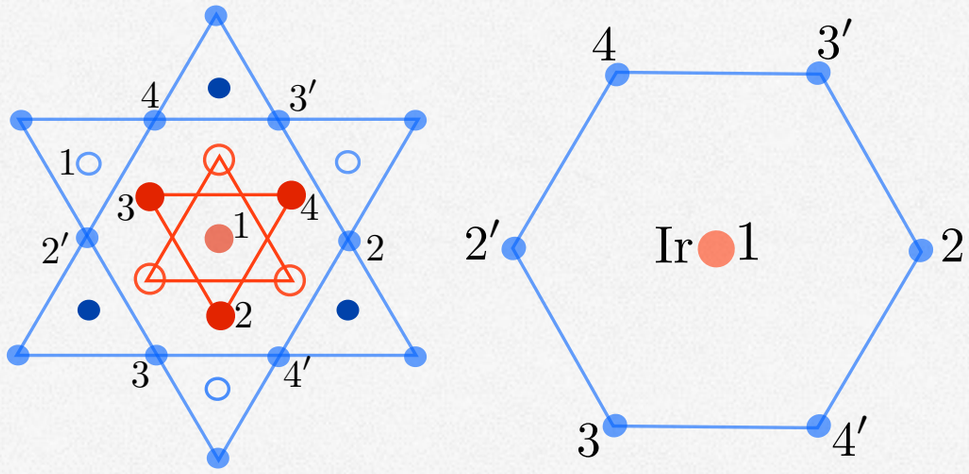

$R_2Ir_2O_7$ on 111 plane

$$\mathcal{H}_{\mathrm{K}}^{(1)} = [c_1\tau_4^z - c_2(\tau_2^z + \tau_3^z)]j_1^x + [c_1\tau_3^z - c_2(\tau_2^z + \tau_4^z)]j_1^y + [c_1\tau_2^z - c_2(\tau_3^z + \tau_4^z)]j_1^z + [2 \leftrightarrow 2', 3 \leftrightarrow 3', 4 \leftrightarrow 4'],$$

Similar for Kramer's doublet

Chen, et al, unpublished

IRIDATE: SOC

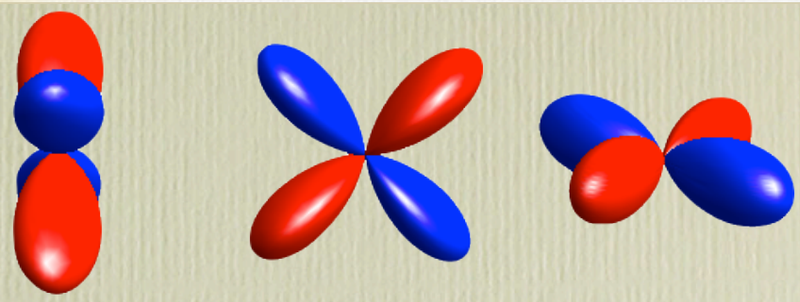

yz xz xy

t_{2g} orbitals

= effective l=1 orbital angular momentum

$$P_{t_{2g}} \boldsymbol{L}_{\ell=2} P_{t_{2g}} = -\boldsymbol{L}_{\ell=1}$$

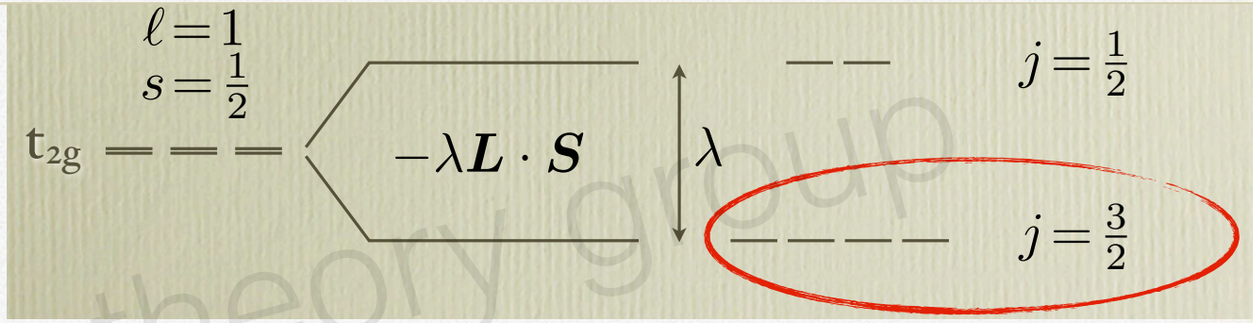

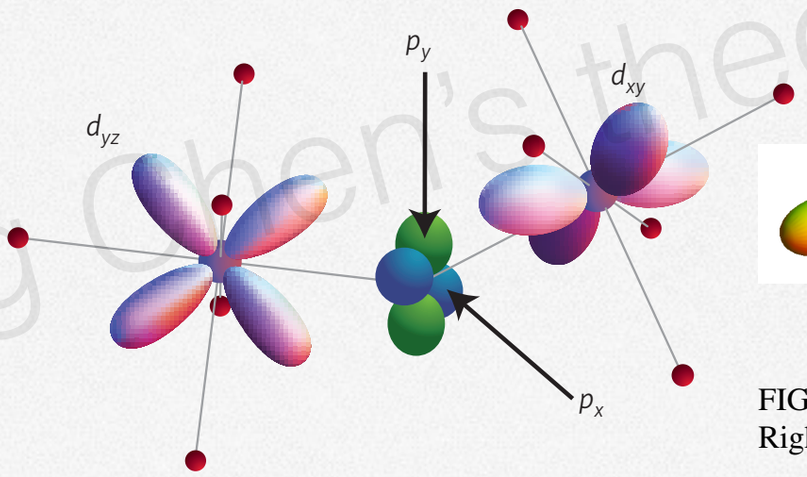

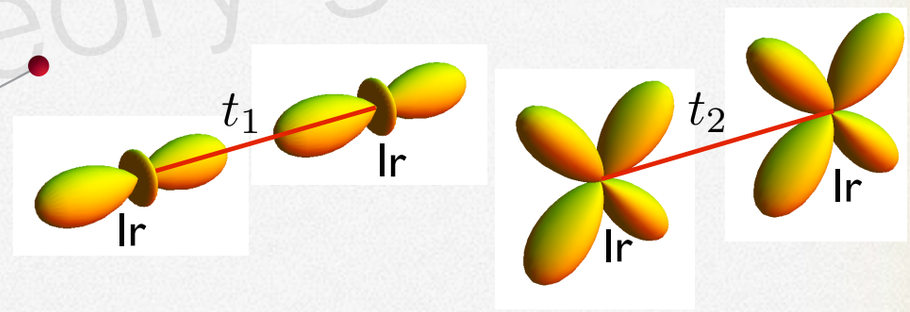

FIG. 4. (Color online) Left: σ-bonding with tunneling amplitude t_1. Right: π-bonding with tunneling amplitude t_2.

Witczak-Krempa et al, 2011
Chen, et al, unpublished

RKKY EXCHANGE

Table I. Curie–Weiss fitting parameters for $R_2Ir_2O_7$.

R	Pr	Nd	Gd	Tb	Dy	Ho	Yb
χ_0 (10^{-3} emu/mol-Ir)	1.6	1.2	0.24	0.33	2.1	3.4	3.3
$p_{\rm eff}$ (obs.)	3.00	3.20	8.18	9.62	10.1	10.3	3.55
$p_{\rm eff}$ (calc.)	3.58	3.62	7.94	9.72	10.63	10.58	4.54
$\theta_{\rm CW}$ (K)	−10	−19	−7.8	−14	−3.5	−0.83	−9.3

Table I. Magnetic properties of $R_2Sn_2O_7$.

R	$\Theta_{\rm CW}$	χ' peak [80 Hz]	magnetic state
Pr	0.32 K [3–20 K]	0.35 K	spin ice
Nd	−0.18 K [2–15 K]	0.93 K	AF ($T_{\rm N} \sim 0.9$ K)
Gd	−6.58 K [50–300 K]	1.0 K	AF ($T_{\rm N} \sim 1.0$ K)
Tb	—	0.87 K	F ($T_{\rm C} \sim 0.87$ K)
Dy	1.69 K [16–40 K]	2.1 K	spin ice
Ho	1.80 K [16–40 K]	1.4 K	spin ice
Er	—	<0.15 K	*the unknown*
Tm	—	none	Van Vleck para.
Yb	0.51 K [2–14 K]	<0.15 K	*the unknown*

Indicate domination of RKKY in some materials

K Matsuhira, *et al*, J. Phys. Soc. Jpn. **76**, 043706 (2007).
S. Nakatsuji, *et al*, Phys. Rev. Lett. **96**, 087204 (2006).
Y. Machida, *et al*, Phys. Rev. Lett. **98**, 057203 (2007).
Y. Machida, *et al*, Nature **463**, 210 (2010).
M. Watahiki, *et al*, J Phys: Conf. Series **320**, 012080 (2011).
M. Sakata, *et al*, Phys. Rev. B **83**, 041102 (2011).
K. Tomiyasu, *et al*, arXiv:1110.6605, unpublished.
K. Matsuhira, *et al*, J Phys: Conf. Series **320**, 012050 (2011).

OUTLINE

- Introduction
- Model Hamiltonian
- Phase diagram
- Experimental relevance

PHASE DIAGRAM

w/o Kondo

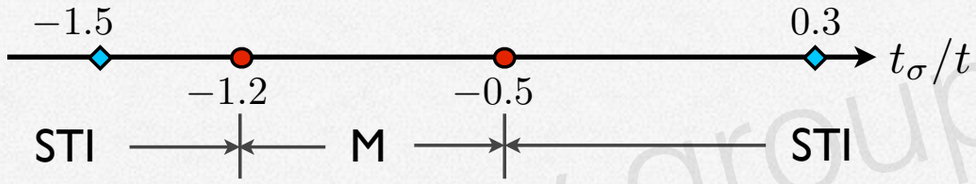

FIG. 2. (Color online) The phase diagram without Kondo coupling. M=metal, STI=strong topological insulator. In this one dimension phase diagram, the circles (dark red) are phase boundaries; the diamonds (light blue) are two cases studied in this paper.

w. Kondo

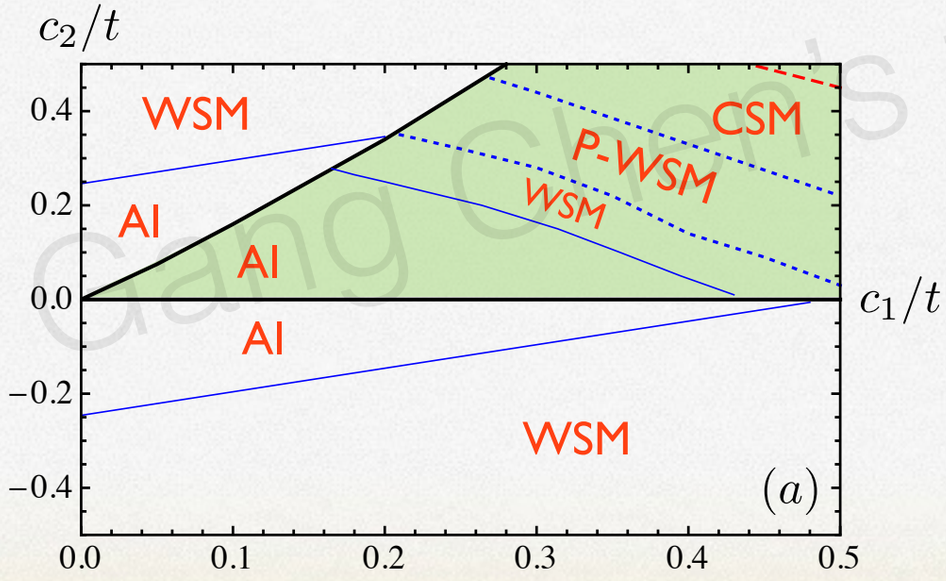

Chen, et al, unpublished

BAND STRUCTURE

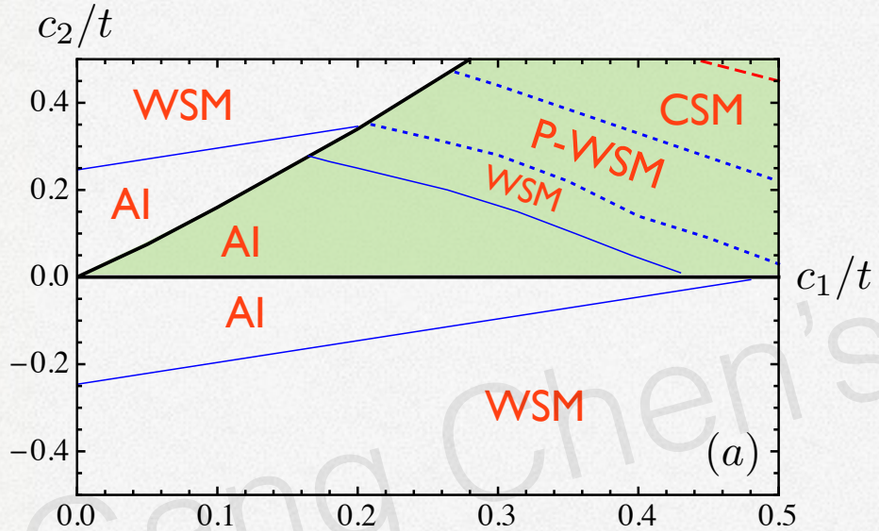

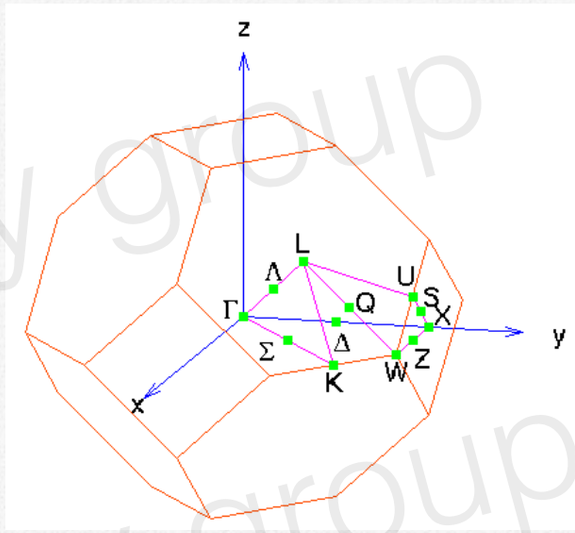

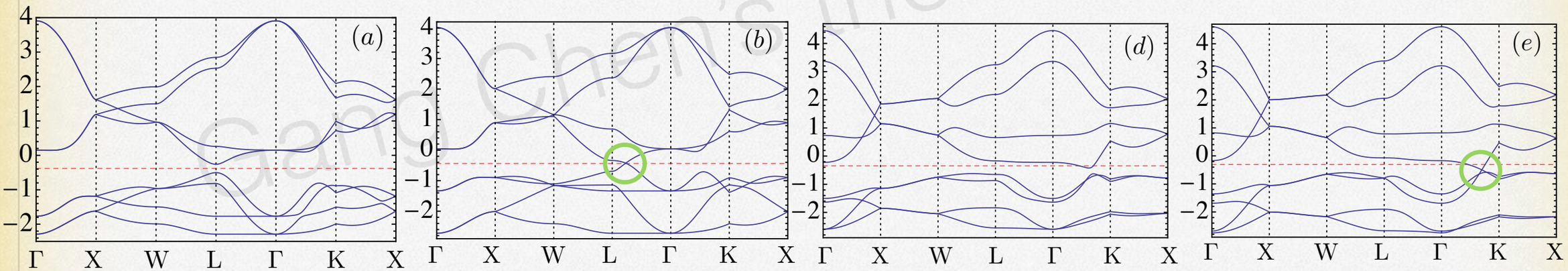

AI *WSM* *P-WSM* *Annihilation of Weyl points*

Chen, et al, unpublished

SURFACE STATES

k.p theory $\mathcal{H}_{\mathrm{WSM}} = E_0 + \mathbf{v}_0 \cdot \mathbf{q} + \sum_i (\mathbf{v}_i \cdot \mathbf{q})\, \sigma_i,$

Chirality $c = sgn[v_1 \cdot (v_2 \times v_3)],$

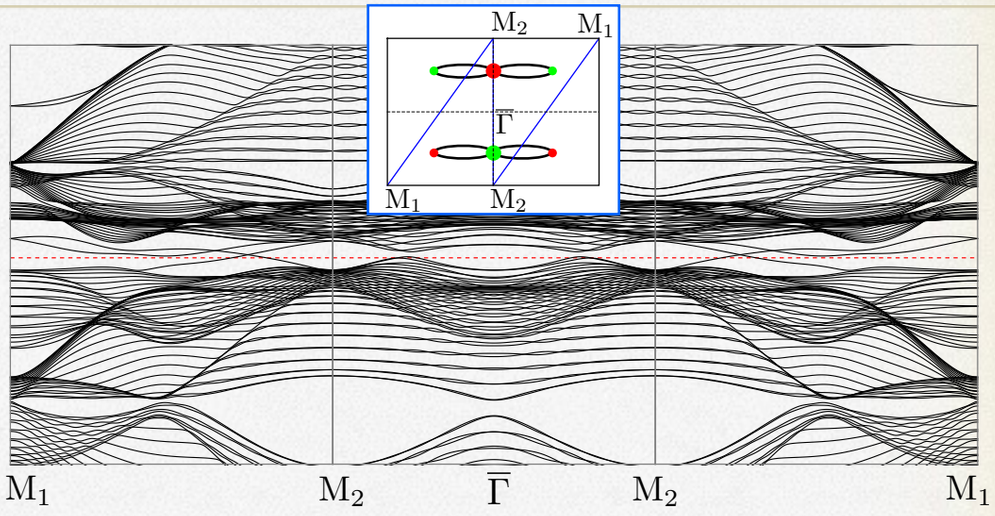

(110) surface plane with 4-in-4-out magnetic order

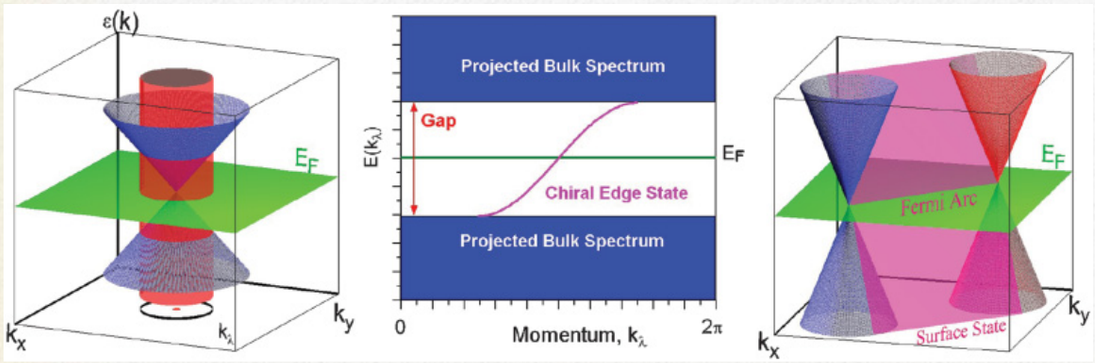

(111) surface plane:BZ

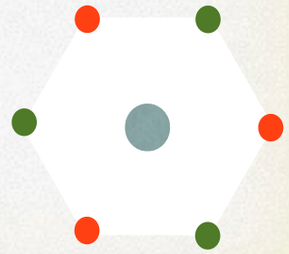

Chen, et al, unpublished

CORRELATION EFFECT

Slave-rotor MFT

$$d_{Ri\alpha} = e^{-i\theta_{Ri}} f_{Ri\alpha} \qquad L_{Ri} = \sum_\alpha f^\dagger_{Ri\alpha} f_{Ri\alpha} - n_d$$

$$H_f = \sum_{Ri\alpha} (\varepsilon_\alpha - \mu - h) f^\dagger_{Ri\alpha} f_{Ri\alpha} + tQ_f \sum_{\substack{\langle Ri, R'i'\rangle \\ \alpha\alpha'}} T^{ii'}_{\alpha\alpha'} f^\dagger_{Ri\alpha} f_{R'i'\alpha'}$$

$$H_\theta = \frac{U}{2} \sum_{Ri} L^2_{Ri} + h(L_{Ri} + n_d) + tQ_\theta \sum_{\langle Ri, R'i'\rangle} e^{i\theta_{Ri} - i\theta_{R'i'}}$$

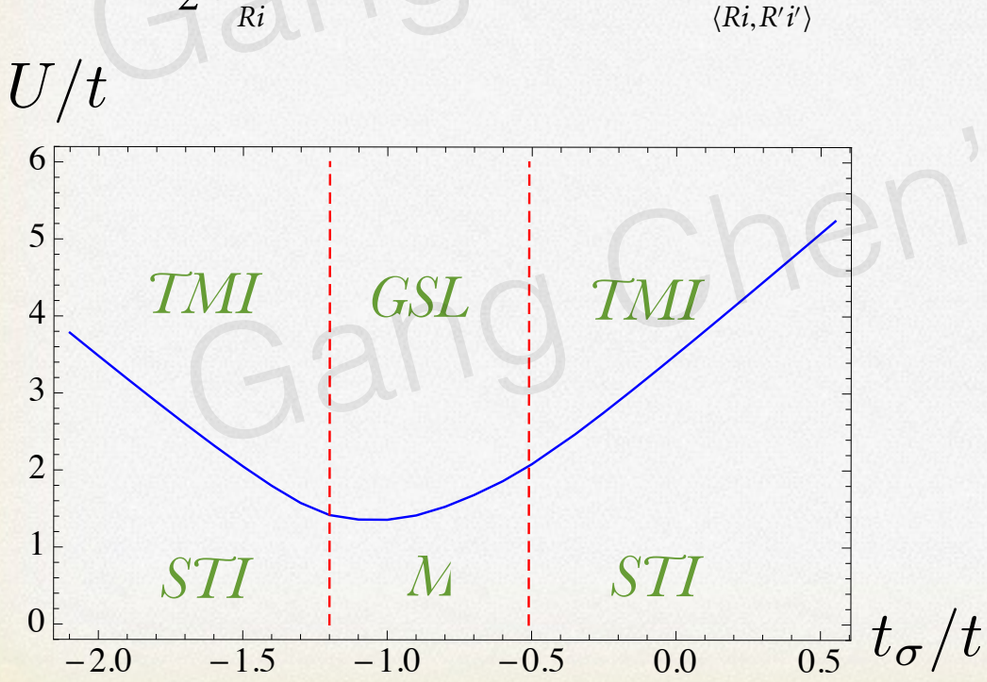

Hartree-Fock MFT

$$\boldsymbol{j}_{Ri} = \sum_{\alpha\beta=\uparrow,\downarrow} d^\dagger_{Ri\alpha} \boldsymbol{\sigma}_{\alpha\beta} d_{Ri\beta}/2$$

$$H_U \to -U \sum_{Ri} (2\langle \boldsymbol{j}_{Ri}\rangle \cdot \boldsymbol{j}_{Ri} - \langle \boldsymbol{j}_{Ri}\rangle^2),$$

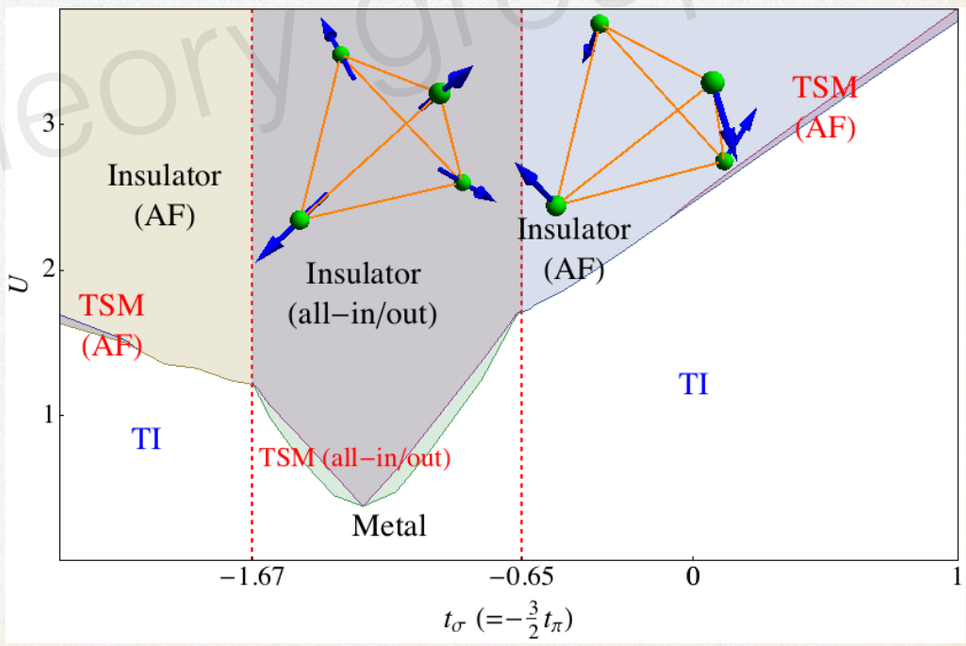

Witczak-Krempa et al, 2011
Chen, et al unpublished

CORRELATION EFFECT

Moving away from the "simple" slave-rotor MFT is non-trivial!

$$H_f = \sum_{Ri\alpha} (\varepsilon_\alpha - \mu - h) f^\dagger_{Ri\alpha} f_{Ri\alpha} + tQ_f \sum_{\substack{\langle Ri, R'i' \rangle \\ \alpha\alpha'}} T^{ii'}_{\alpha\alpha'} f^\dagger_{Ri\alpha} f_{R'i'\alpha'} + H_{kondo}$$

$$H_\theta = \frac{U}{2} \sum_{Ri} L^2_{Ri} + h(L_{Ri} + n_d) + tQ_\theta \sum_{\langle Ri, R'i' \rangle} e^{i\theta_{Ri} - i\theta_{R'i'}}$$

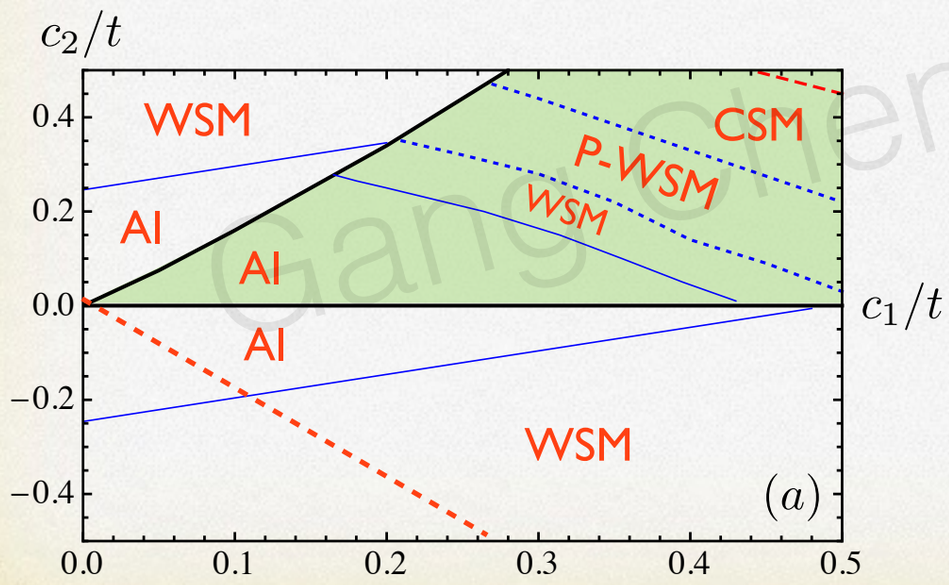

Determine phase diagram energetically

Possibility of first order Mott-transition

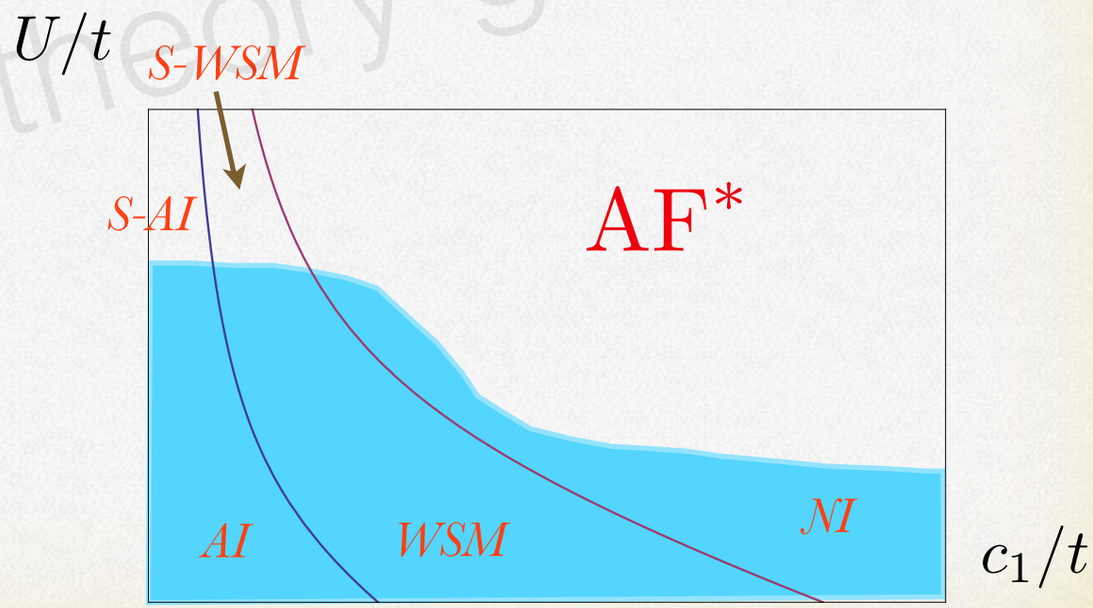

Chen, et al, unpublished

DOUBLE WEYL SEMIMETAL

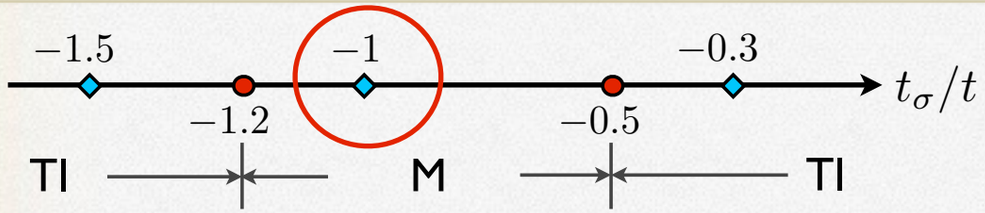

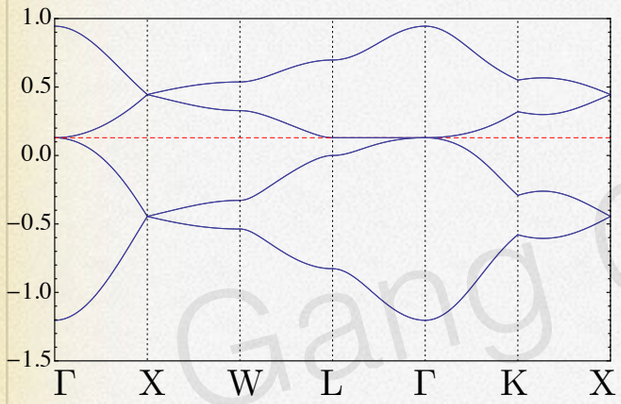

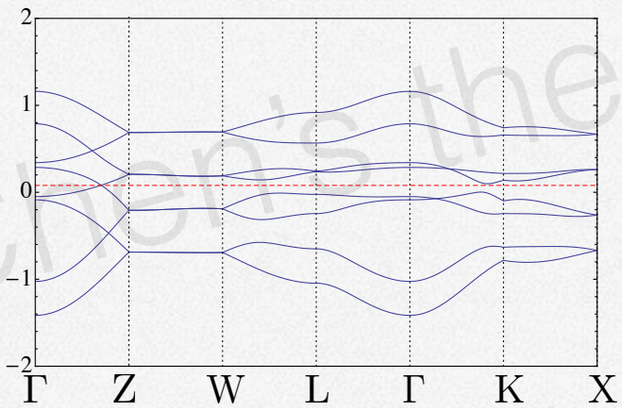

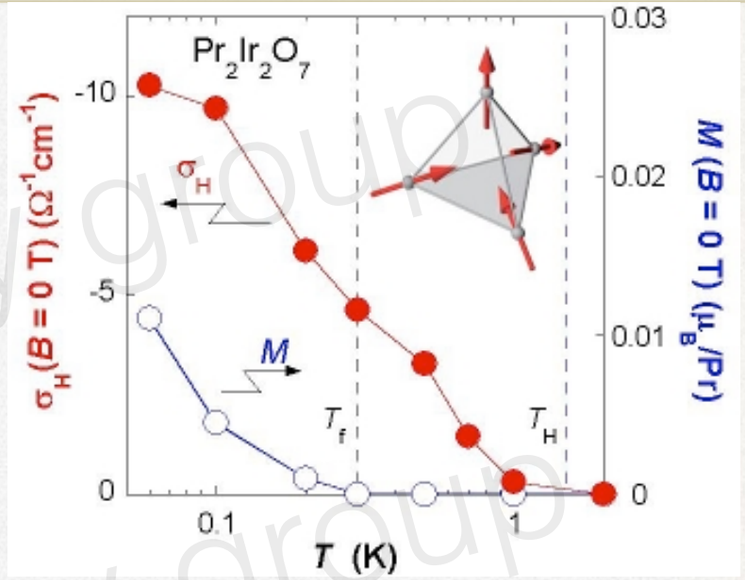

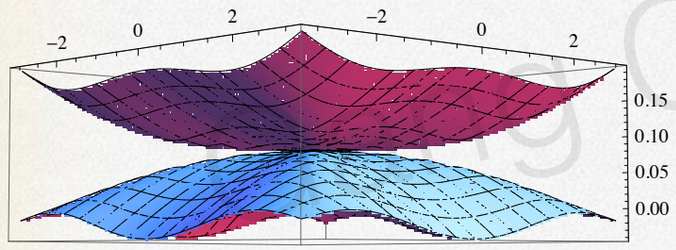

kx-ky plane

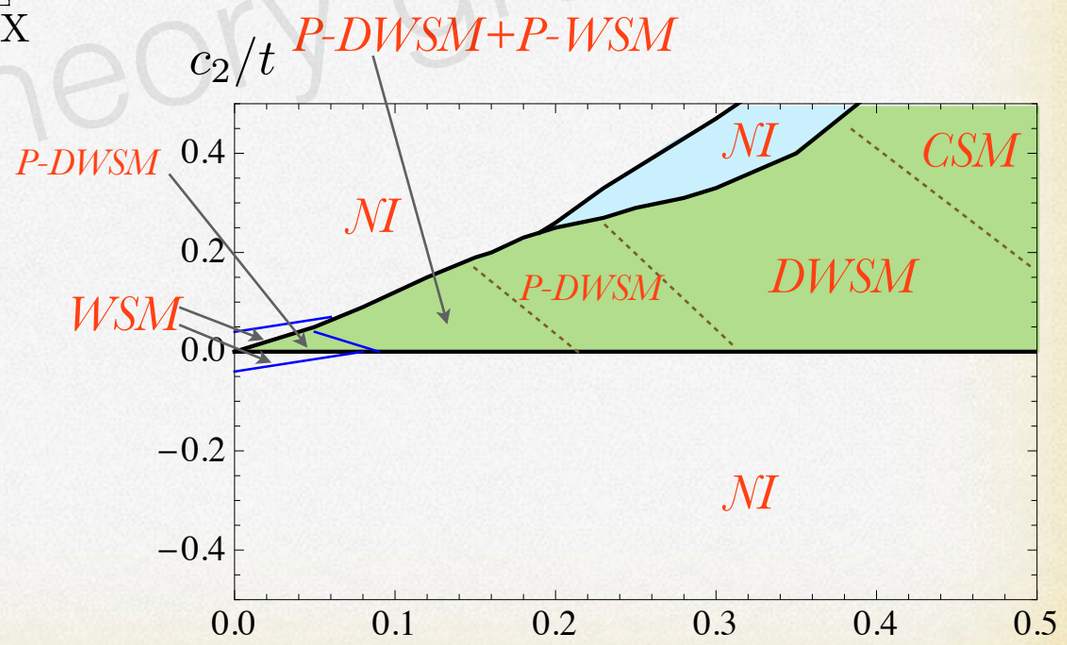

Symmetry protected quadratic band touching
Analogous to bilayer graphene!

Chen, et al unpublished

Surface state for double Weyl semi-metal

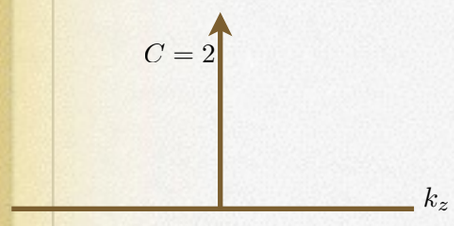

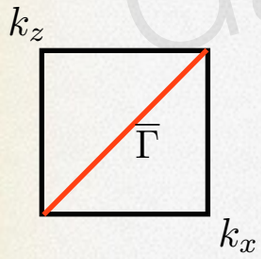

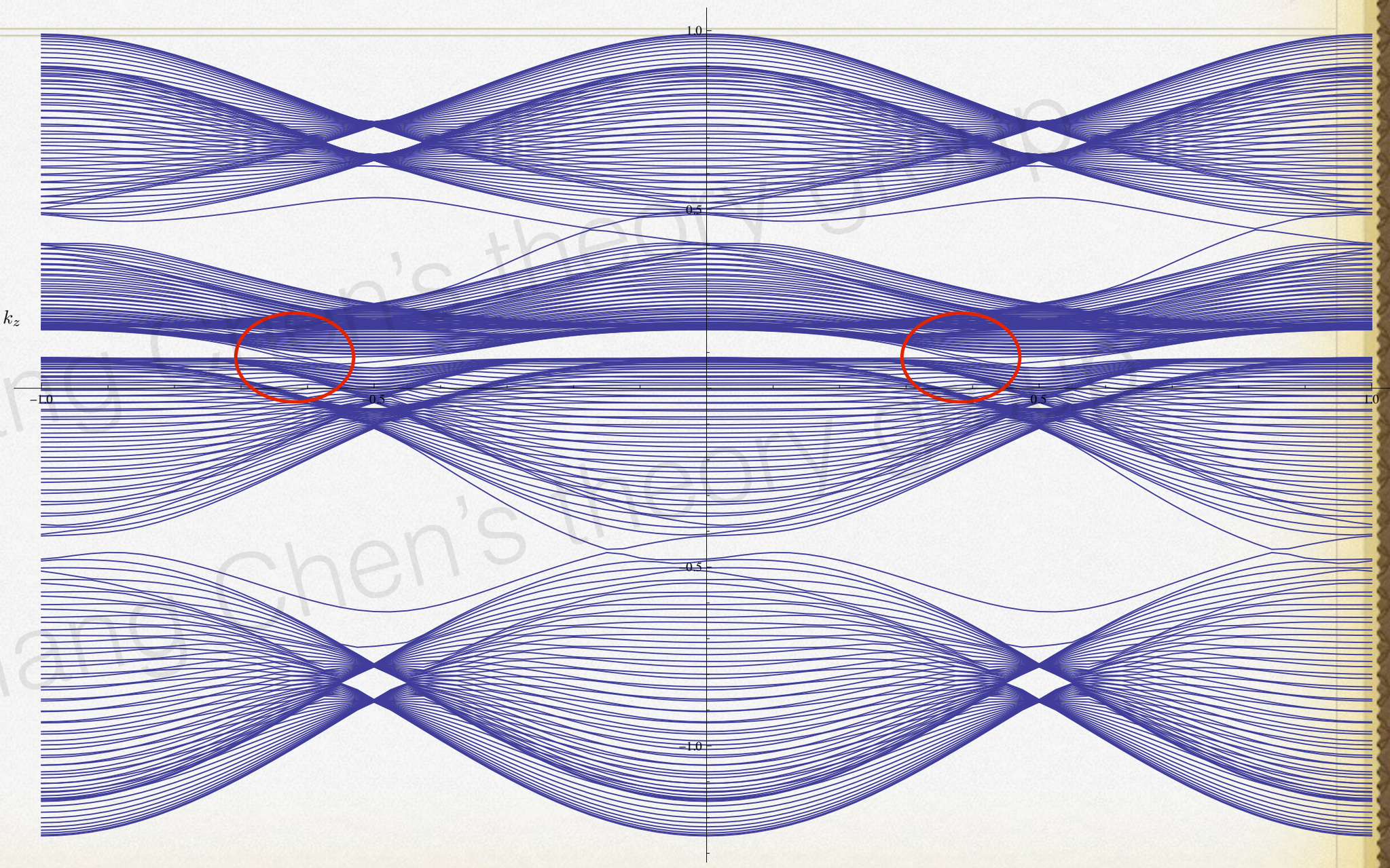

ANOMALOUS HALL EFFECT

WSM

$$\vec{\nu}_{\text{node}} = \sum_i (-)^{\xi_i} \vec{\mathbf{P}}_i .$$

$$\sigma_{ij} = \frac{e^2}{2\pi h} \epsilon_{ijk} \nu_k .$$

"4-in 4-out" $\boldsymbol{\nu} = \mathbf{0}$

"2-in 2-out" $\boldsymbol{\nu} = (0, 0, 8k_z) \pmod{4\pi}.$

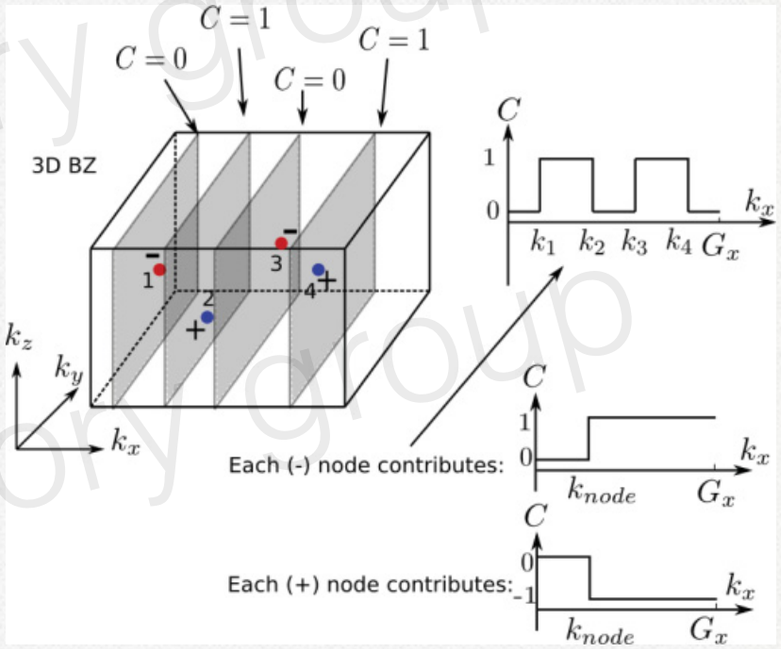

FIG. 3. (Color online) Schematic illustration of the proof of the general formula (3).

Yang, et al 2011

OUTLINE

- Introduction
- Model Hamiltonian
- Phase diagram
- Experimental relevance

Compound	Metal/Insulator	Magnetism
$Pr_2Ir_2O_7$	Metal	Spin freezing at 0.12K[35–37]
$Tb_2Ir_2O_7$	MIT	Unknown[18]
$Ho_2Ir_2O_7$	MIT	Unknown[18]
$Nd_2Ir_2O_7$	MIT at 36K	LRO[38–40]
$Sm_2Ir_2O_7$	MIT at 117K	Magnetic order at MIT [34]
$Gd_2Ir_2O_7$	MIT	Unknown[18]
$Dy_2Ir_2O_7$	MIT at 134K	No LRO down to 0.1K [41]
$Yb_2Ir_2O_7$	I	Unknown[18]

$Nd_2Ir_2O_7$ AI and Pressure induced WSM?

Nd-Neodymium

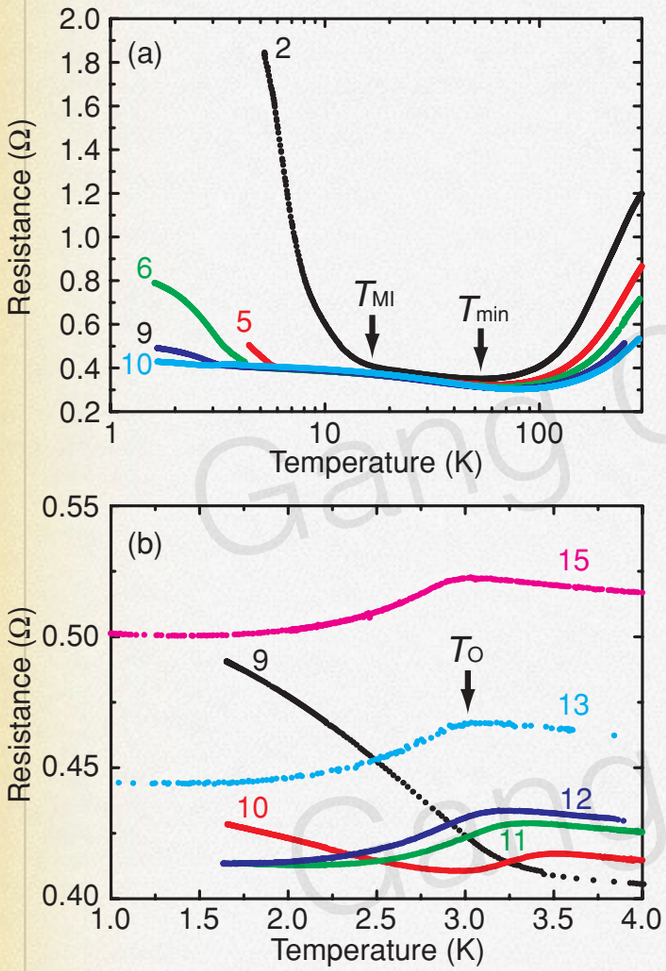

$Nd_2Ir_2O_7$

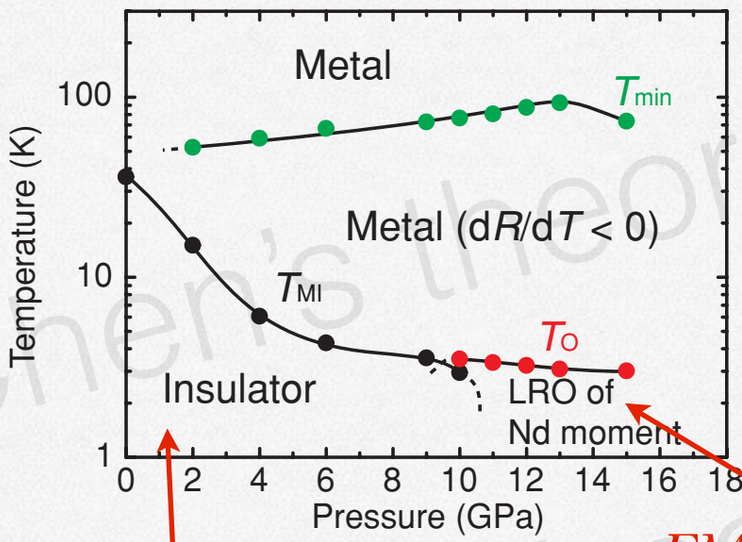

FIG. 3. (Color online) Phase diagram for $Nd_2Ir_2O_7$.

q=0 4-in 4-out spin config

FM metal with q=0 2-in 2-out spin config

clean, non-interaction
w coulomb
w impurity

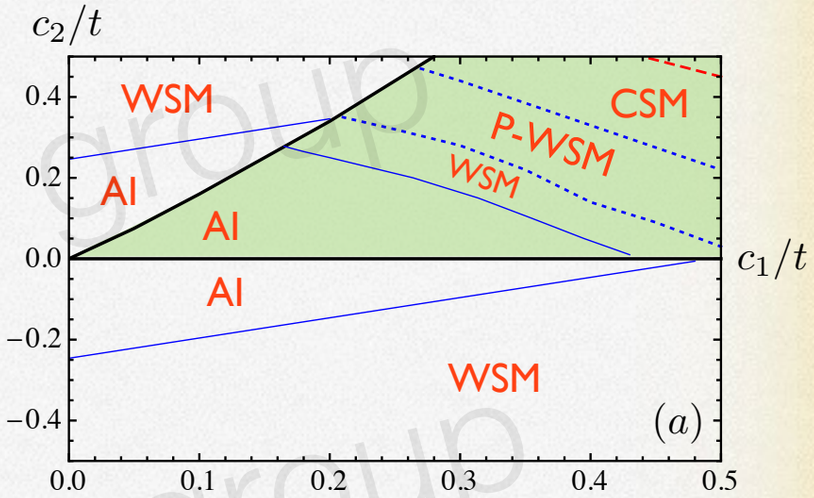

$$\sigma_0(\omega) = N\frac{e^2}{12h}\frac{|\omega|}{v_F}$$

$$\sigma_{\rm dc} \sim e^2\left(\frac{\epsilon^2}{v_F^3}\right)v_F^2\tau \sim \frac{k_BT}{\alpha}$$ power law insulator

$$\mathrm{Re}\,\sigma(\omega,T) \propto \sigma_0 f(\omega/T^2)$$

Sakata, et al 2011
Tomiyasu, et al 2011

$Nd_2Ir_2O_7$ AI and Pressure induced WSM?

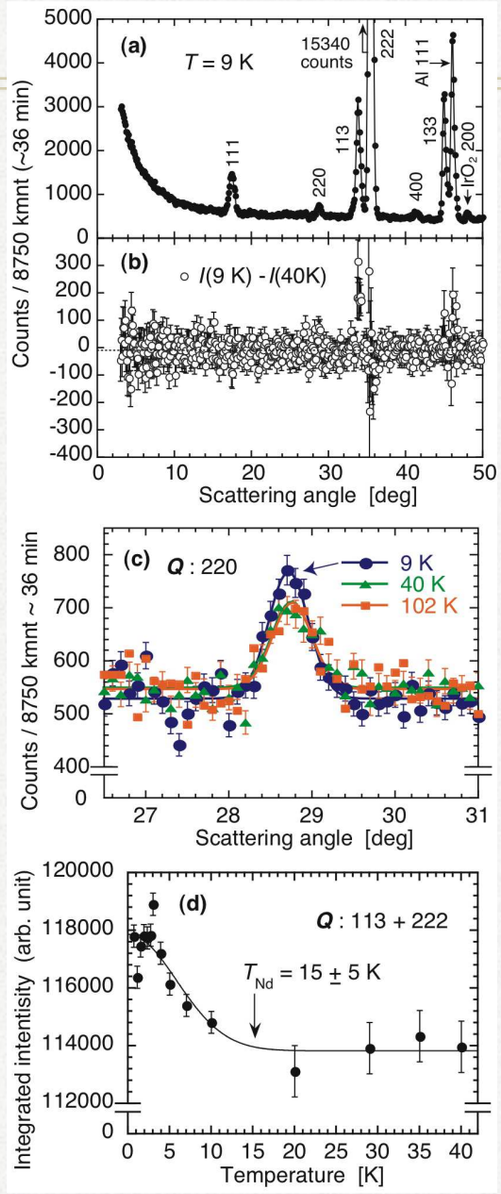

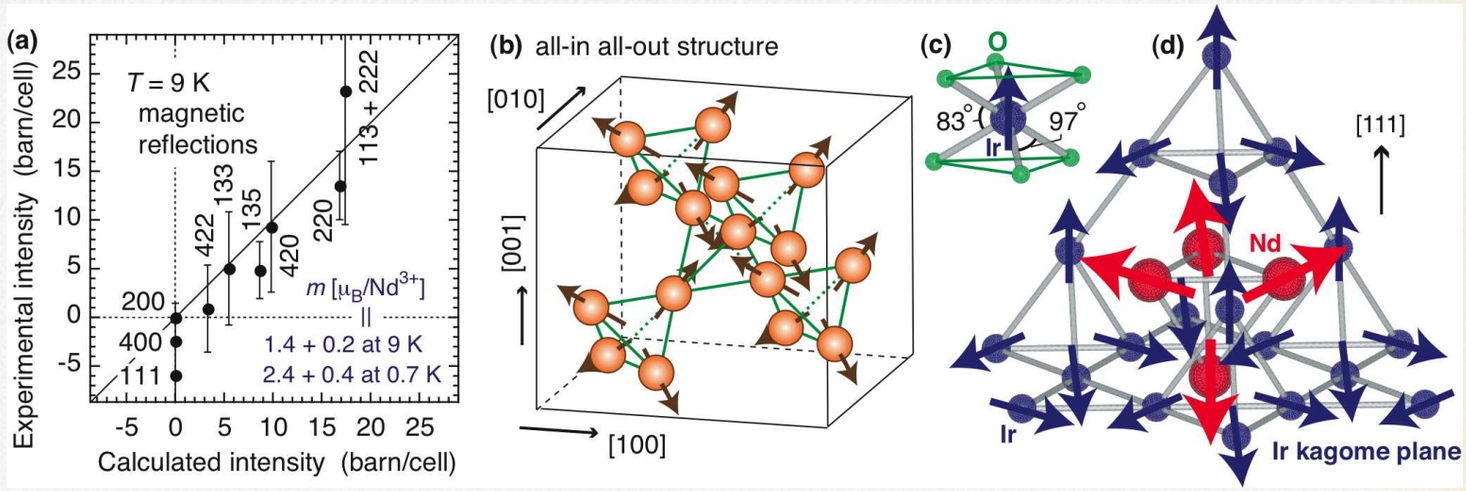

FIG. 1: (Color online) Measured neutron diffraction data for powder $Nd_2Ir_2O_7$. (a) Diffraction data measured at 9 K. (b) Diffraction data obtained by subtracting the 40 K data from the 9 K data (a). (c) Bragg reflection lines measured around the (220) reciprocal lattice point at 9 K, 40 K, and 102 K. (d) Temperature dependence of summation of the integrated intensities 113 and 222. In (a), (c), and (d), all the lines are a guide to the eye.

Sakata, et al 2011
Tomiyasu, et al 2011

$Sm_2Ir_2O_7$: another WSM?

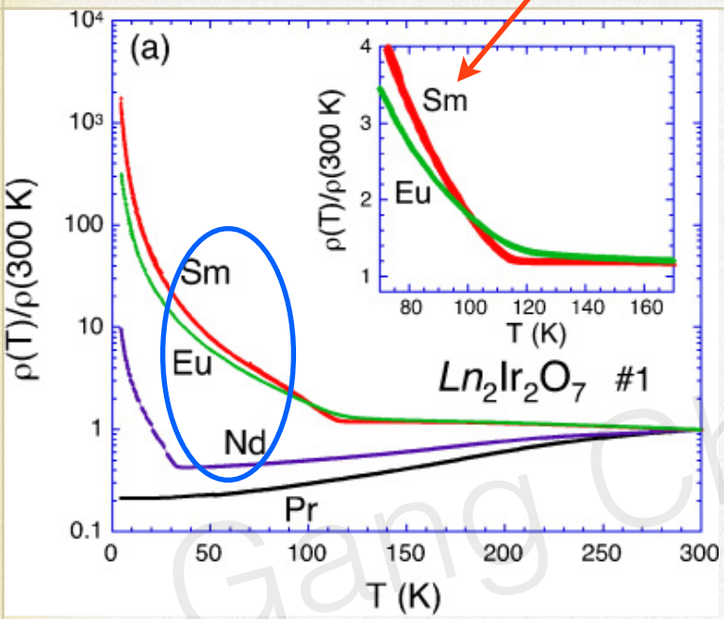

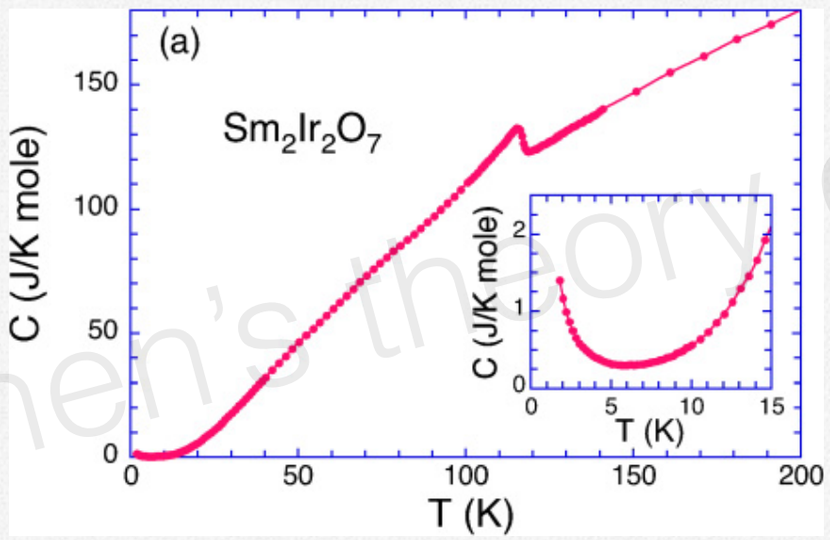

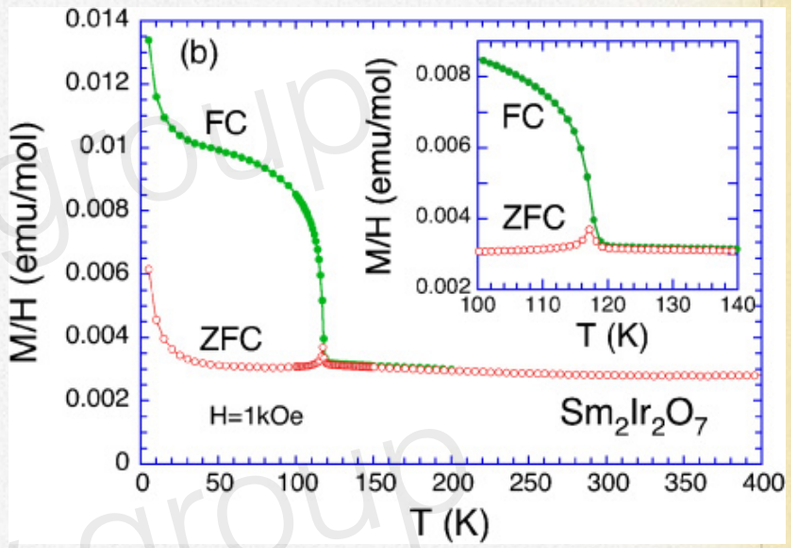

clean, non-interaction
w coulomb
w impurity

$$\sigma_0(\omega) = N\frac{e^2}{12h}\frac{|\omega|}{v_F}$$

$$\sigma_{\rm dc} \sim e^2\left(\frac{\epsilon^2}{v_F^3}\right)v_F^2\tau \sim \frac{k_BT}{\alpha}$$ power law insulator

$$\mathrm{Re}\,\sigma(\omega,T) \propto \sigma_0 f(\omega/T^2)$$

K Matsuhira, *et al*, J. Phys. Soc. Jpn. **76**, 043706 (2007).
S. Nakatsuji, *et al*, Phys. Rev. Lett. **96**, 087204 (2006).
Y. Machida, *et al*, Phys. Rev. Lett. **98**, 057203 (2007).
Y. Machida, *et al*, Nature **463**, 210 (2010).
M. Watahiki, *et al*, J Phys: Conf. Series **320**, 012080 (2011).
M. Sakata, *et al*, Phys. Rev. B **83**, 041102 (2011).
K. Tomiyasu, *et al*, arXiv:1110.6605, unpublished.
K. Matsuhira, *et al*, J Phys: Conf. Series **320**, 012050 (2011).

AXIONIC POLARITON

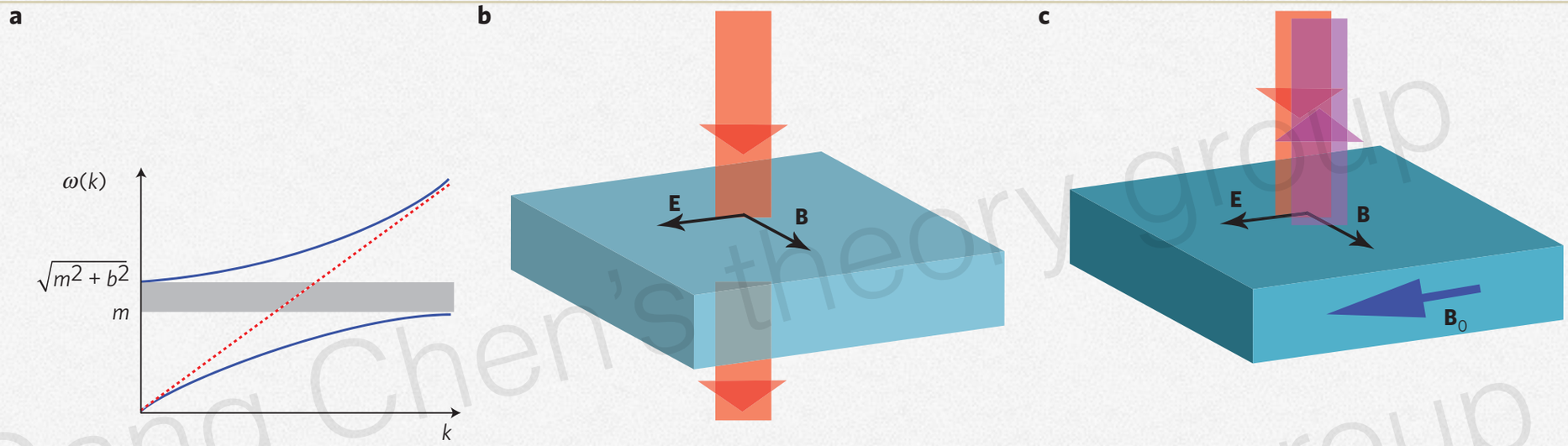

Figure 2 | Axionic polariton and ATR experiment. a, The dispersion of the axionic polariton. The grey area indicates the forbidden band between frequencies m and $\sqrt{m^2+b^2}$ (see text), within which light cannot propagate in the sample. The red dotted line shows the bare photon dispersion $\omega = c'k$. **b**, Set-up for the ATR experiment. Without an external magnetic field, the incident light can transmit through the sample. **c**, When an external magnetic field is applied parallel to the electric field of light, the incident light will be totally reflected if its frequency lies within the forbidden band.

Axion electrodynamics

$$\begin{aligned}\mathcal{S}_{\text{tot}} &= \mathcal{S}_{\text{Maxwell}} + \mathcal{S}_{\text{topo}} + \mathcal{S}_{\text{axion}} \\ &= \frac{1}{8\pi}\int \mathrm{d}^3x\mathrm{d}t\left(\epsilon\mathbf{E}^2 - \frac{1}{\mu}\mathbf{B}^2\right) + \frac{\alpha}{4\pi^2}\int \mathrm{d}^3x\mathrm{d}t(\theta_0+\delta\theta)\mathbf{E}\cdot\mathbf{B} \\ &\quad + g^2 J\int \mathrm{d}^3x\mathrm{d}t[(\partial_t\delta\theta)^2 - (v_i\partial_i\delta\theta)^2 - m^2\delta\theta^2] \qquad (4)\end{aligned}$$

Kerr effect and Faraday rotation will also be useful tools

R. Li, etc, natphys 2010
W. Tse, etc 2010

$Pr_2Ir_2O_7$ is a DWSM?

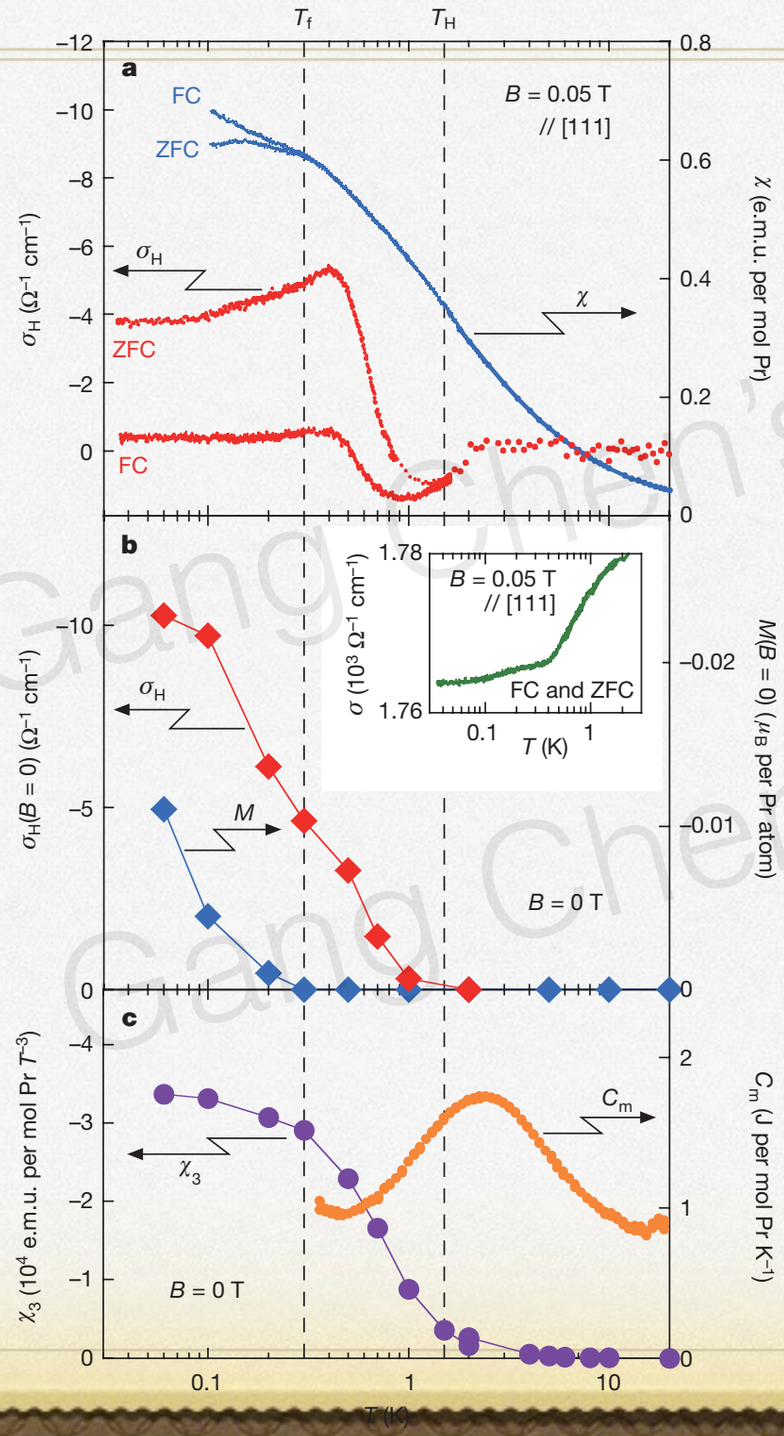

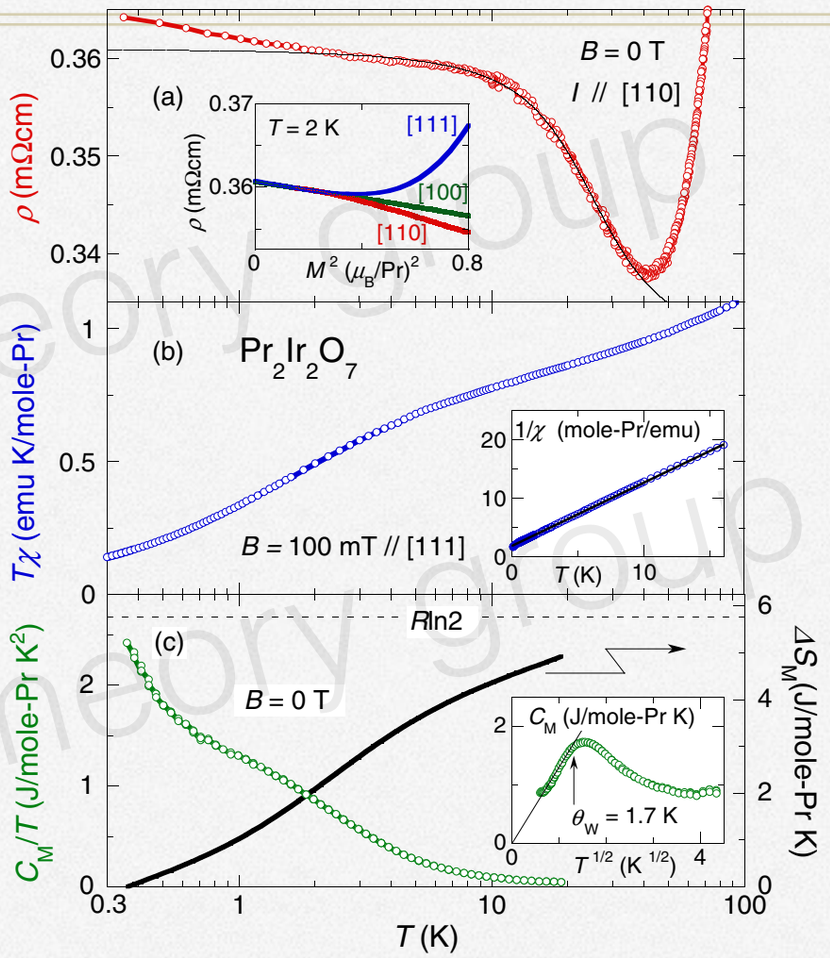

FIG. 4 (color online). (a) Low T resistivity $\rho(T)$ vs ln$T$. Inset: transverse magnetoresistance vs the square of the magnetization M^2 along various axes. (b) Effective Curie constant $C(T) \equiv T\chi(T)$ vs ln$T$. Inset: inverse susceptibility $\chi^{-1}(T)$. (c) Magnetic part of the specific heat divided by temperature C_M/T (left axis) and the entropy $\Delta S_M(T) \equiv S(T) - S(0.35\ \mathrm{K})$ (right axis) as a function of ln$T$. The horizontal broken line indicates $\Delta S_M(T) = R\ln 2$. Inset: C_M as a function of $T^{1/2}$.

FUTURE DIRECTIONS

- Influence of monopole events in spin ice on the axion dynamics
- Orbital effect of magnetic field in double Weyl semimetal
- The transport of double Weyl semimetal
- Correlation effects: fractionalized phase, nontrivial gauge dynamics

SUMMARY

- We proposed a Kondo-coupling model for R2Ir2O7
- We found several topological phases: WSM, P-WSM, DWSM, AI and even spinon versions of these phases
- The phases are likely to be relevant to current experiments

Frustrated quantum critical theory of putative spin-liquid phenomenology in 6H-B-$Ba_3NiSb_2O_9$

- Introduction
- Minimal model + Phase diagram
- Predictions

Collaborator: M. Hermele & L. Radzihovsky

ArXiv: 1201.2182

High pressure sequence of $Ba_3NiSb_2O_9$ structural phases: new $S = 1$ quantum spin-liquids based on Ni^{2+}

J. G. Cheng,[1] G. Li,[2] L. Balicas,[2] J. S. Zhou,[1] J. B. Goodenough,[1] Cenke Xu,[3] and H. D. Zhou[2,*]

[1] *Texas Materials Institute, University of Texas at Austin, TX 78712, USA*
[2] *National High Magnetic Field Laboratory, Florida State University, Tallahassee, FL 32306-4005, USA*
[3] *Department of Physics, University of California, Santa Barbara, California 93106, USA*

(Dated: August 16, 2011)

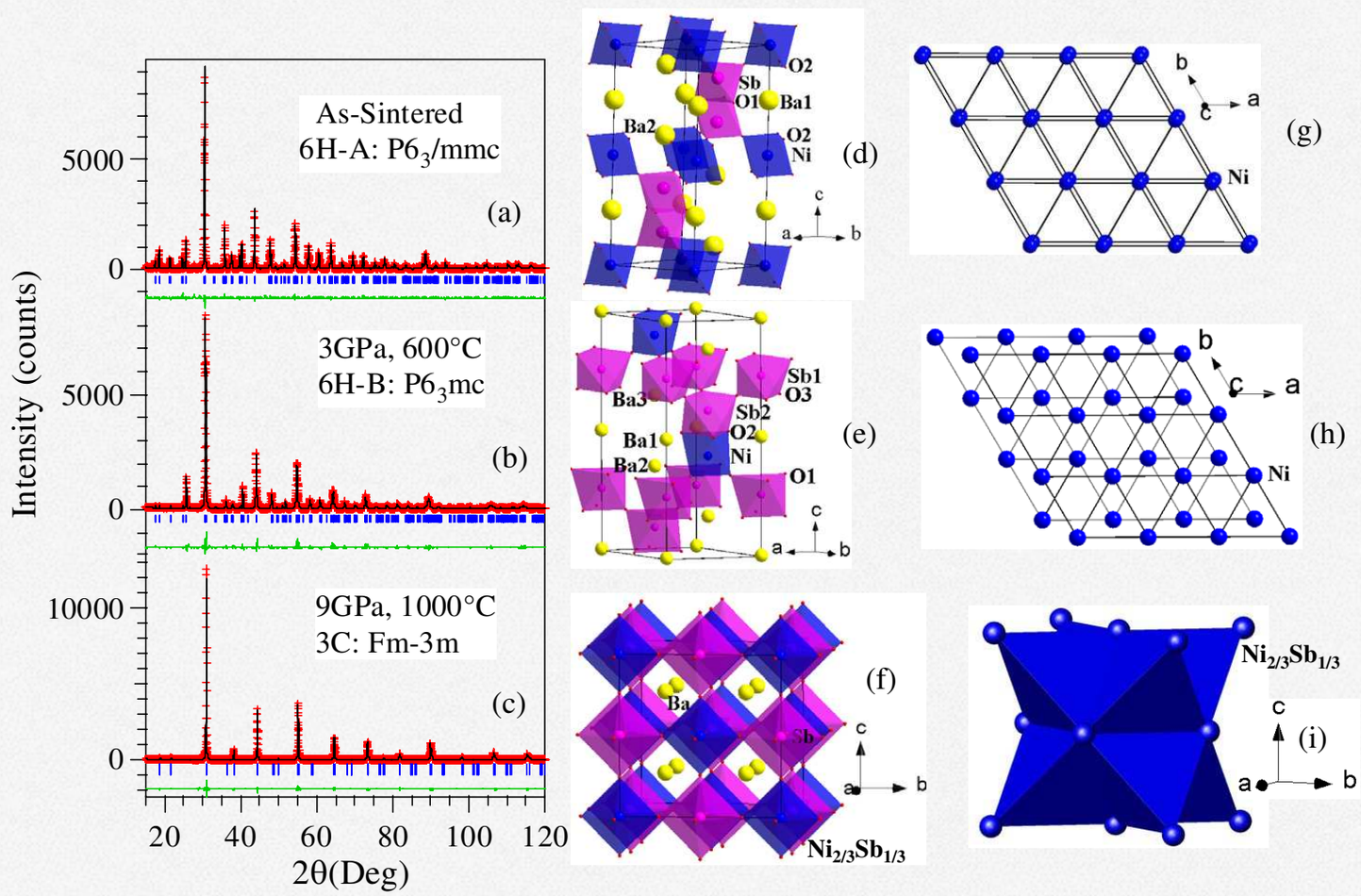

FIG. 1: (Color online) Powder XRD patterns (crosses) at 295 K for the $Ba_3NiSb_2O_9$ polytypes: (a) 6H-A, (b) 6H-B, and (c) 3C. Solid curves are the best fits obtained from Rietveld refinements using FullProf. Schematic crystal structures for the $Ba_3NiSb_2O_9$ polytypes: (d) 6H-A, (e) 6H-B, and (f) 3C, red octahedra represents Sb(M') site and blue octahedra represents $Ni_{2/3}Sb_{1/3}$(M) site. Magnetic lattices composed of Ni^{2+} ions for the $Ba_3NiSb_2O_9$ polytypes: (g) 6H-A, (h) 6H-B, and (i) 3C.

Cheng et al, PRL 107, 19720 (2011)

Constant χ and linear-T C_v: Quantum spin liquid?

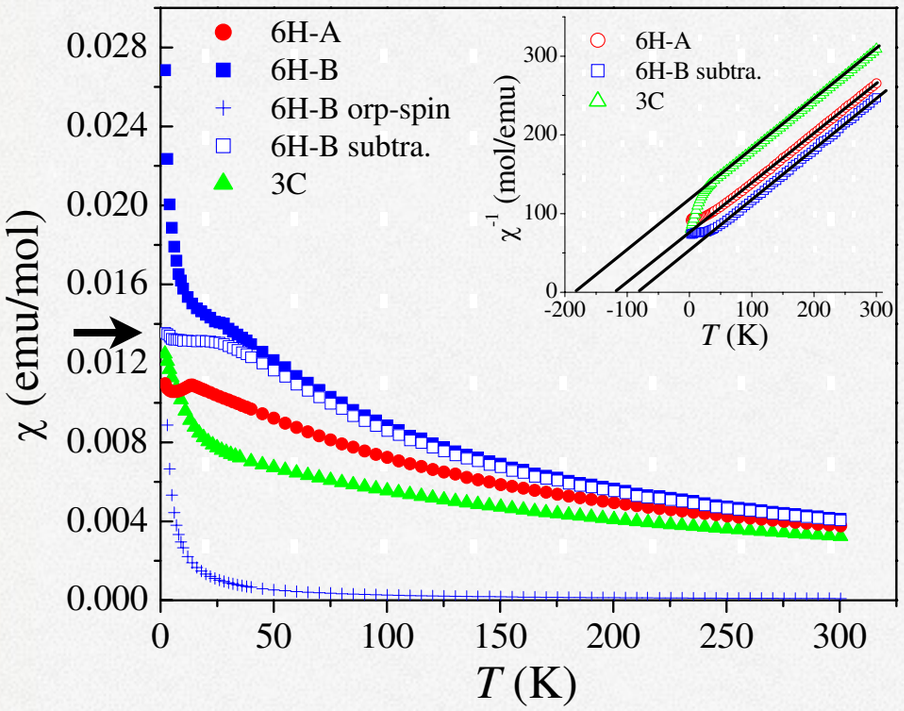

FIG. 2: (Color online) (a) Temperature dependencies of the DC magnetic susceptibility (χ) for the $Ba_3NiSb_2O_9$ polytypes. Inset: Temperature dependencies of $1/\chi$. The solid lines on $1/\chi$ data represent Curie-Weiss fits. For 6H-B phase, χ (open squares) is obtained by subtracting 1.7% Ni^{2+} orphan spin's contribution (crosses) from the as measured data (solid squares).

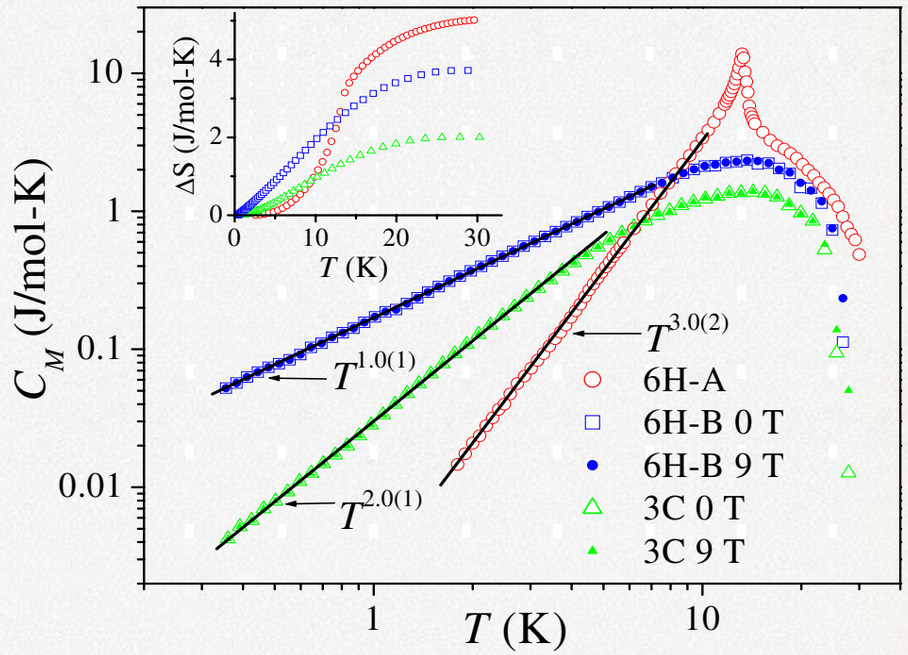

FIG. 3: (Color online) (a) Temperature dependencies for the magnetic specific heat (C_M) for all three $Ba_3NiSb_2O_9$ polytypes. Solid lines are the fits as described in the main text. Inset: variation in magnetic entropy ΔS below 30 K.

MIT theory

$$H = \sum_{\langle ij \rangle} [J \vec{S}_i \cdot \vec{S}_j + K(\vec{S}_i \cdot \vec{S}_j)^2] + D \sum_i (S_i^z)^2,$$

$$\vec{S}_i = -\mathrm{i} \vec{f}_i^\dagger \times \vec{f}_i, \qquad \vec{f}_i^\dagger \cdot \vec{f}_i = 1.$$

$$|x\rangle = \mathrm{i}(|1\rangle - |-1\rangle)/\sqrt{2}$$

$$|y\rangle = (|1\rangle + |-1\rangle)/\sqrt{2}$$

$$|z\rangle = -\mathrm{i}|0\rangle$$

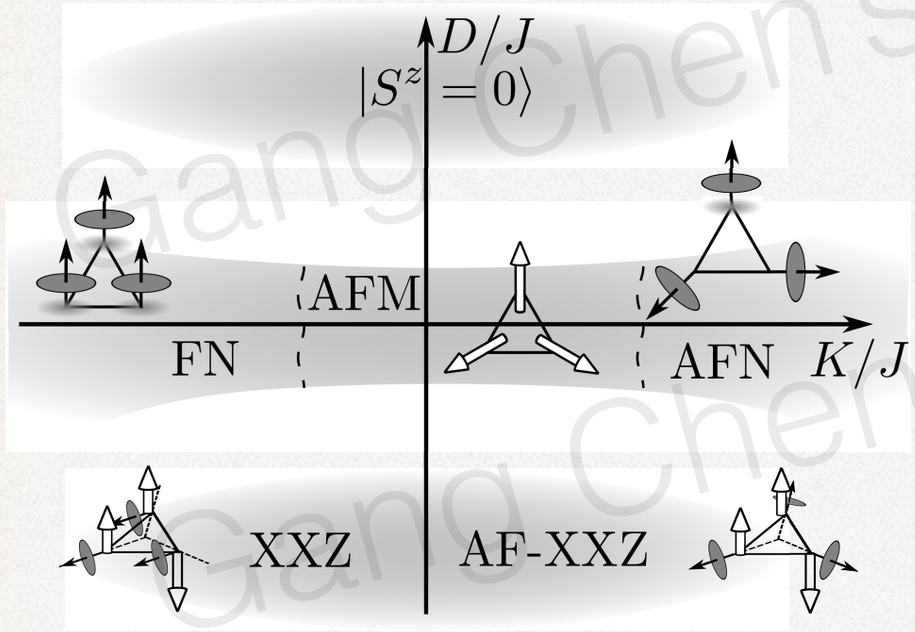

FIG. 1. Schematic representation of the ground state in different limits of the Hamiltonian (1). White arrows represent average spin; arrows with discs indicate the director of the nematic order parameter. Details are discussed in the text.

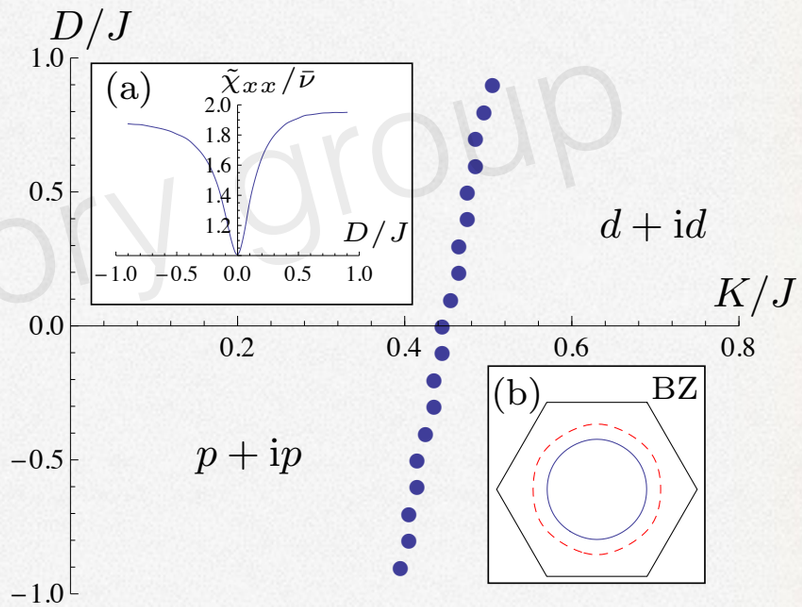

FIG. 2. The phase boundary between SL GS's with $p+\mathrm{i}p$ and $d+\mathrm{i}d$ pairing. (a) The spin susceptibility $\tilde{\chi}_{xx}$ in the $d+\mathrm{i}d$ phase as a function of D/J for $K/J = 0.55$. The susceptibility is normalized by the average density of states, $\bar{\nu} = (\nu_x + \nu_z)/2$, where ν_x is calculated without the gap. (b) Gapped (dashed red line) and ungapped (blue line) Fermi surfaces of x, y, and z-fermions for $K/J = 0.55$, $D/J = 0.8$.

ArXiv 1108.3070

UCSB theory

$$\hat{S}_i^\mu = \frac{1}{2} \sum_{\alpha,\beta=\uparrow,\downarrow} \sum_{a=1,2} f^\dagger_{\alpha,a,i} \sigma^\mu_{\alpha\beta} f_{\beta,a,i}.$$

$$\hat{n}_i = \sum_{a=1,2} \sum_{\alpha=\uparrow,\downarrow} f^\dagger_{\alpha,a,i} f_{\alpha,a,i} = 2,$$

$$\hat{\tau}^\mu = \sum_{\alpha,a,b} f^\dagger_{\alpha,a,i} \tau^\mu_{ab} f_{\alpha,b,i} = 0.$$

$$\mathrm{U(1)}_c \ : \ f_{\alpha,a,i} \to e^{i\theta_i} f_{\alpha,a,i};$$

$$\mathrm{SU(2)}_o \ : \ f_{\alpha,a,i} \to [e^{i\vec{\theta}_i \cdot \vec{\tau}/2}]_{ab} f_{\alpha,b,i}.$$

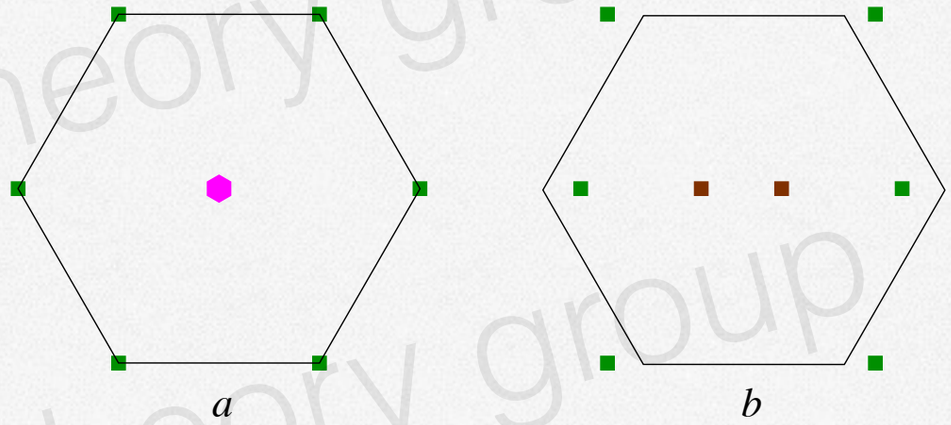

FIG. 1: a, The spin liquid we are considering contains a quadratic band touching at $\vec{k} = 0$ (hexagon), and Dirac points (squares) at the corners of the Brillouin zone. b, with a nonzero and small nematic order $N_1 > 0$, the quadratic band touching is split into two Dirac points, and the locations of the other Dirac points are shifted.

ArXiv 1110.3328

Crystal structure

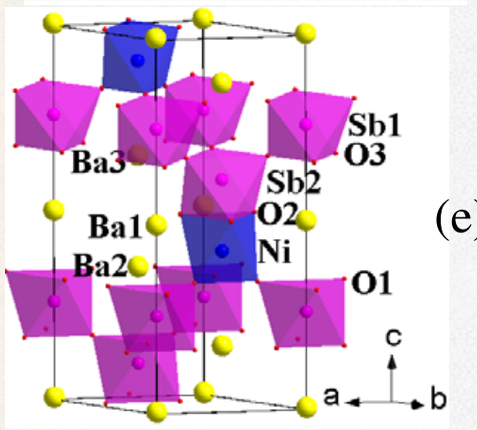

(e)

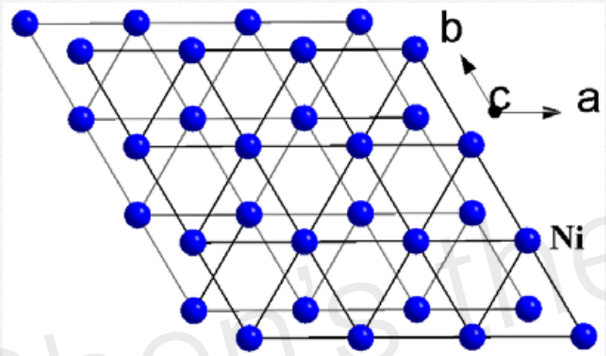

(h)

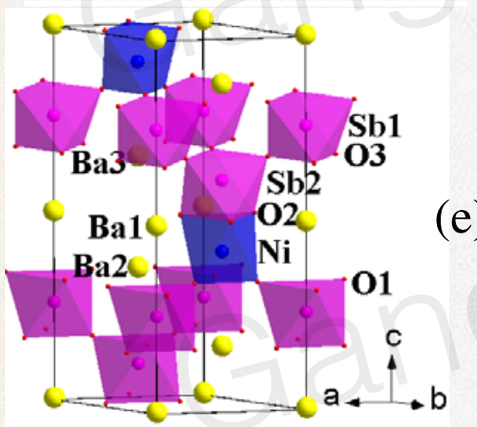

(e)

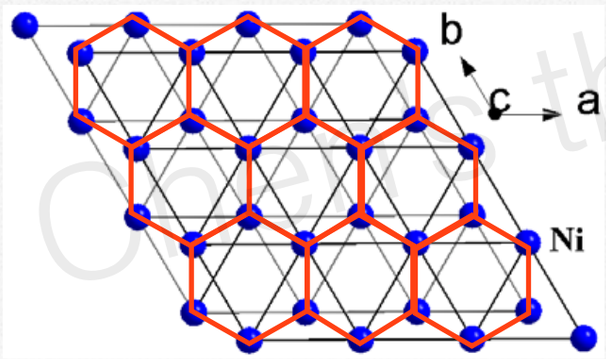

(h)

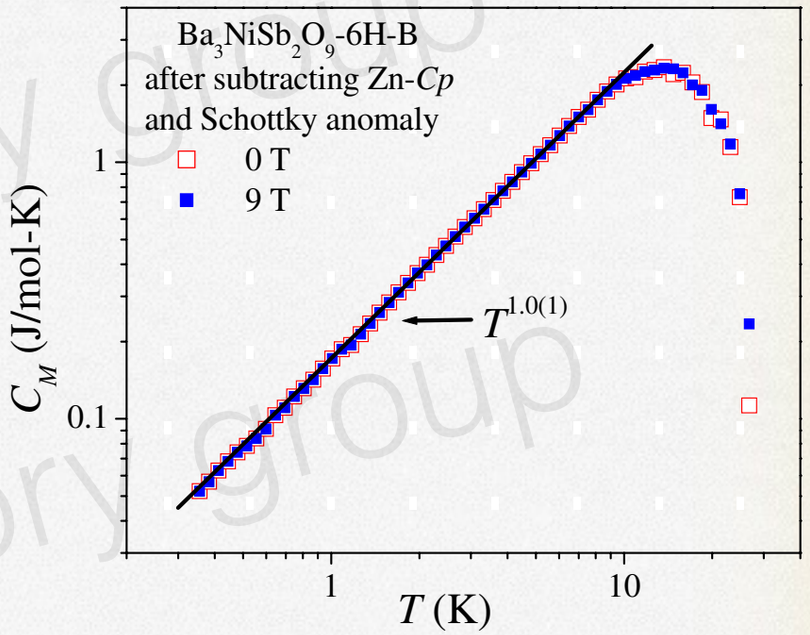

$$\mu_{\text{eff}} \sim 3.54\ \mu_B$$

$$\Theta_{CW} = -75.6K$$

Model

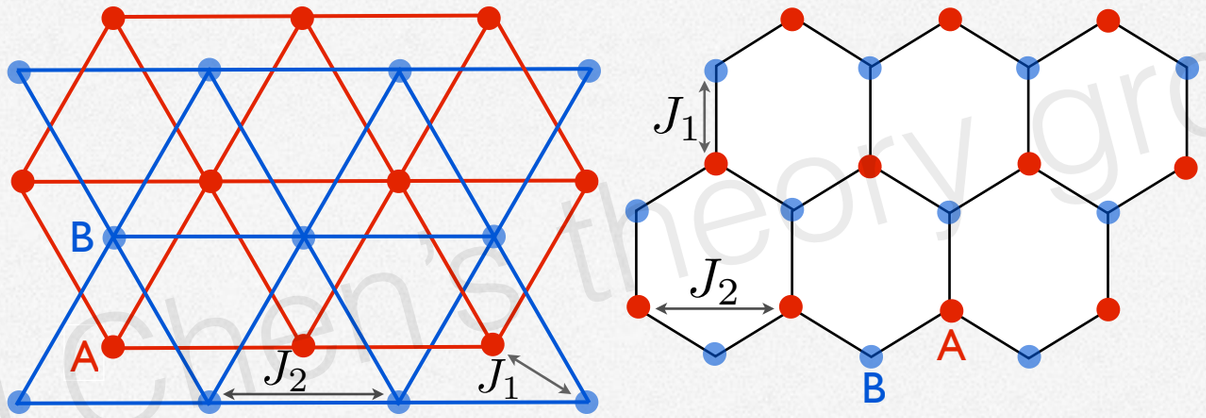

FIG. 1. (Color online) The bilayer triangular lattice (left) is equivalent to a single layer honeycomb lattice (right). J_1, J_2 are interlayer and intralayer exchange, respectively.

$$\mathcal{H}_{\text{ex}} = J_1 \sum_{\langle ij\rangle \in \text{AB}} \mathbf{S}_i \cdot \mathbf{S}_j + J_2 \sum_{\langle ij\rangle \in \text{AA or BB}} \mathbf{S}_i \cdot \mathbf{S}_j,$$

$$\mathcal{H}_{\text{ani}} = D \sum_i (S_i^z)^2,$$

Phase diagram

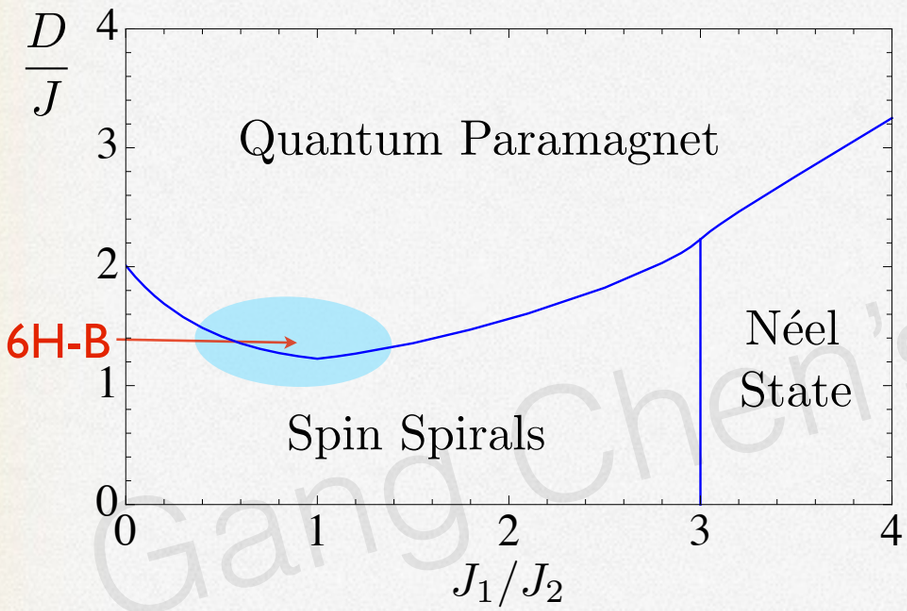

$$J \equiv J_1 + J_2$$

Quantum order-by-disorder

$$\sum_{\{\mathbf{b}\}} \cos(\mathbf{q}_\perp \cdot \mathbf{b}) = (\frac{J_1}{J_2})^2 - 3,$$

$$\mathbf{q}_\perp = \left(0, \frac{2}{\sqrt{3}} \cos^{-1}\left((\frac{J_1}{2J_2})^2 - \frac{5}{4}\right)\right), \text{ if } 1 < \frac{J_1}{J_2} < 3$$

$$\mathbf{q}_\perp = \left(2\cos^{-1}(\frac{J_1}{2J_2} + \frac{1}{2}), \frac{2\pi}{\sqrt{3}}\right), \qquad \text{if } \frac{J_1}{J_2} < 1,$$

Weiss mean field theory

$$\mathbf{S}_{\mathrm{A}}(\mathbf{r}) = M[\cos(\mathbf{q}\cdot\mathbf{r})\hat{x} + \sin(\mathbf{q}\cdot\mathbf{r})\hat{y}],$$
$$\mathbf{S}_{\mathrm{B}}(\mathbf{r}) = M[\cos(\mathbf{q}\cdot\mathbf{r}+\phi)\hat{x} + \sin(\mathbf{q}\cdot\mathbf{r}+\phi)\hat{y}].$$

$$M = \sqrt{2(1 - D/D_c)}$$

$$\chi_0^{\perp} = \frac{2\mu_0(g\mu_B)^2}{D + 12J}$$

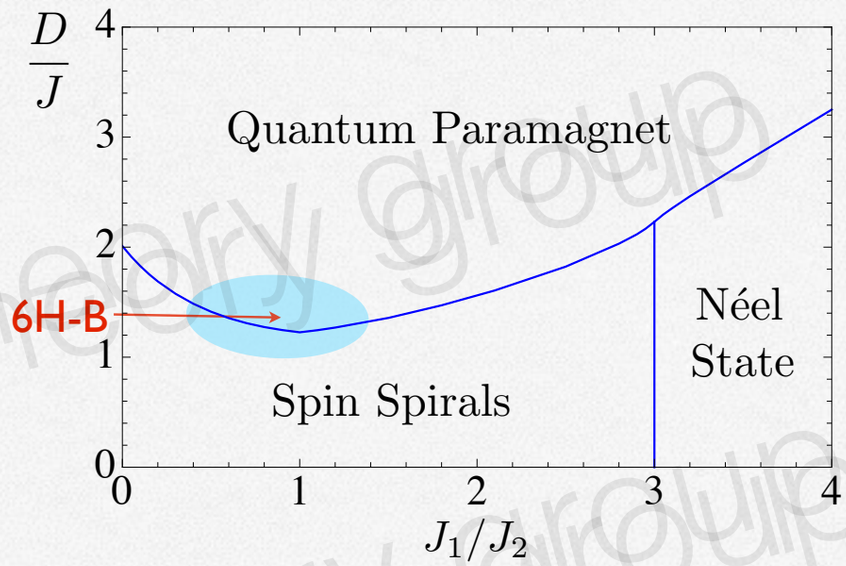

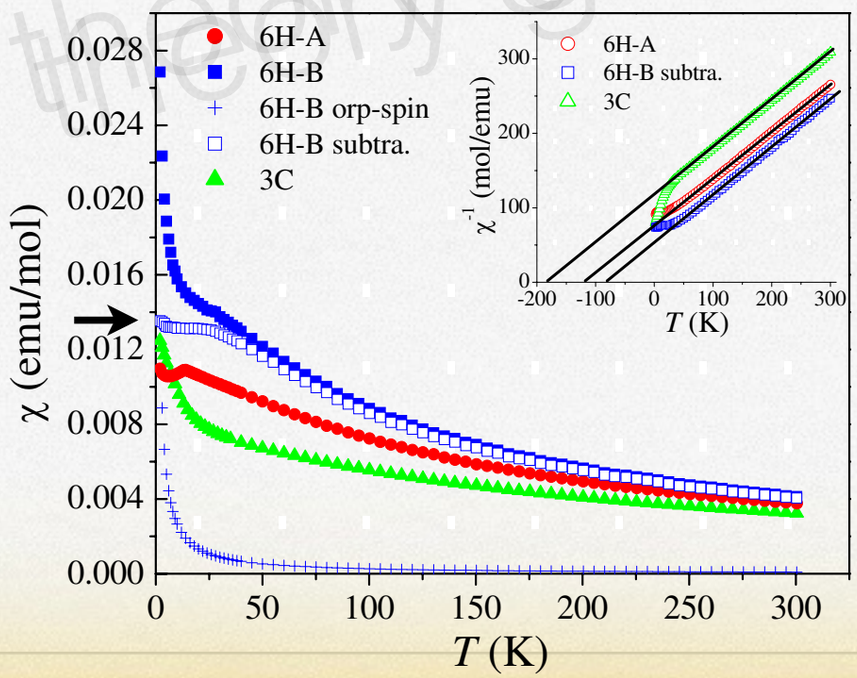

Map to rotor model: MFT from paramagnetic side

$$S_i^z \to n_i \text{ and } S_i^+ \to \sqrt{2}e^{i\phi_i}, \qquad [\phi_i, n_j] = i\delta_{ij}.$$

$$\mathcal{H}_{\text{rotor}} = \frac{1}{2}\sum_{ij} J_{ij}[2\cos(\phi_i - \phi_j) + n_i n_j] + \sum_i D n_i^2.$$

$$\mathcal{Z} = \int \mathcal{D}\Phi \prod_i \delta(|\Phi_i|^2 - 1) e^{-S} \qquad (11)$$

with

$$\rightarrow \quad \mathcal{Z} = \int \mathcal{D}\Phi \mathcal{D}\lambda\, e^{-S - i\sum_i \lambda_i (|\Phi_i|^2 - 1)}.$$

$$\mathcal{S} = \int_\tau \sum_{\mathbf{k}} (4D\mathbb{I} + 2\mathcal{J}_{\mathbf{k}})^{-1}_{\mu\nu} \partial_\tau \Phi^*_{\mu,\mathbf{k}} \partial_\tau \Phi_{\nu,-\mathbf{k}} + \sum_{ij} J_{ij} \Phi_i^* \Phi_j$$

$$s_\pm(\mathbf{k}) = \sum_{\{\mathbf{b}\}} J_2 \cos(\mathbf{k}\cdot\mathbf{b}) \pm |J_1(1 + e^{ik_z}) \sum_{\{\mathbf{a}\}} e^{i\mathbf{k}\cdot\mathbf{a}}|$$

Saddle-point equation

$$\sum_{i=\pm} \int_{\mathbf{k}} \frac{2D + s_i(\mathbf{k})}{\epsilon_i(\mathbf{k})} \coth(\beta\epsilon_i(\mathbf{k})/2) = 2,$$

$$\epsilon_\pm(\mathbf{k}) = \sqrt{(4D + 2s_\pm(\mathbf{k}))(\Delta(T) + s_\pm(\mathbf{k}))}.$$

$$i\lambda_i = \beta\Delta(T)$$

Low-E spin excitation at the QCP

$J_1 > J_2$ $J_1 = J_2$

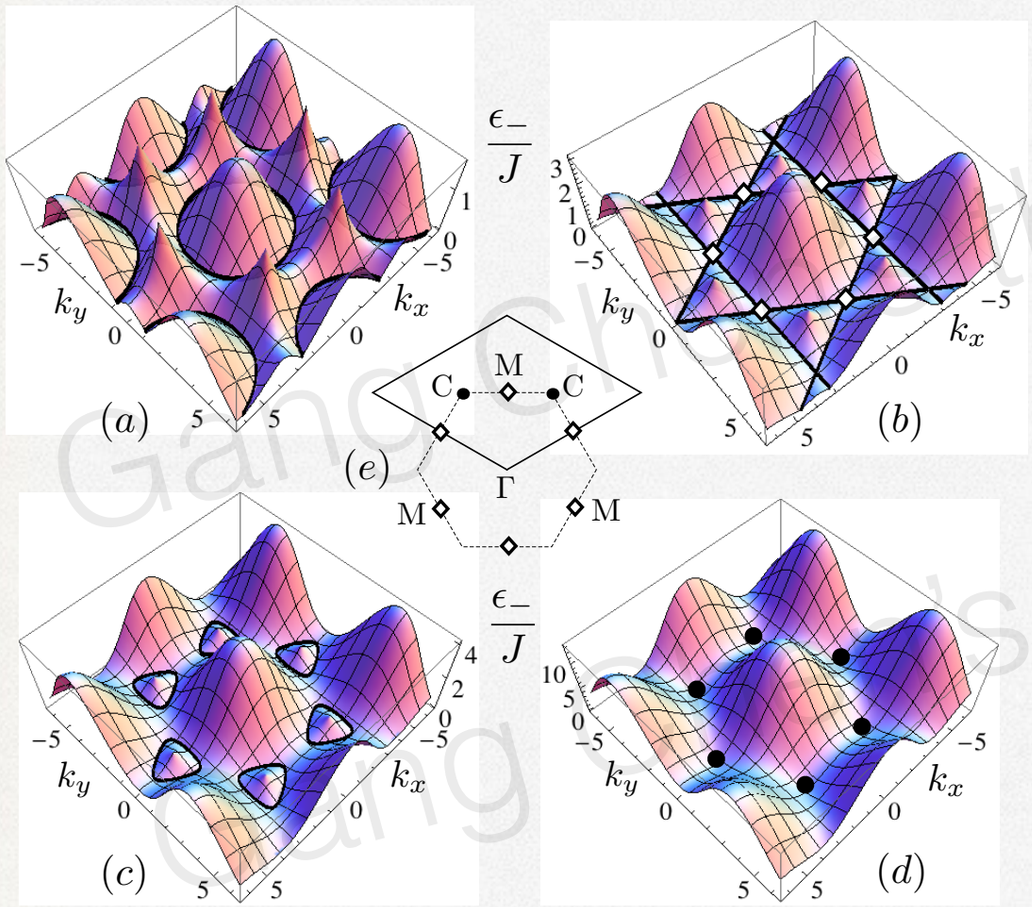

$J_1 < J_2$ $J_1 = 0$

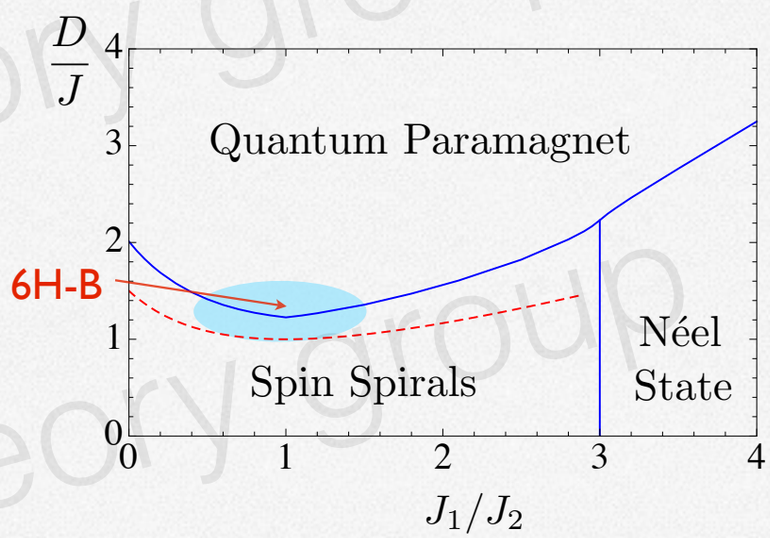

FIG. 2. (Color online) Zero-temperature phase diagram determined from the SPE in Eq. (13). Shaded region (in blue) is the expected parameter regime for the 6H-B compound. Dashed (red) curve indicates the location where $D = \Delta_0/2$, which is important in the discussion of T-linear $C_v(T)$ below. $J \equiv J_1 + J_2$.

Specific heat

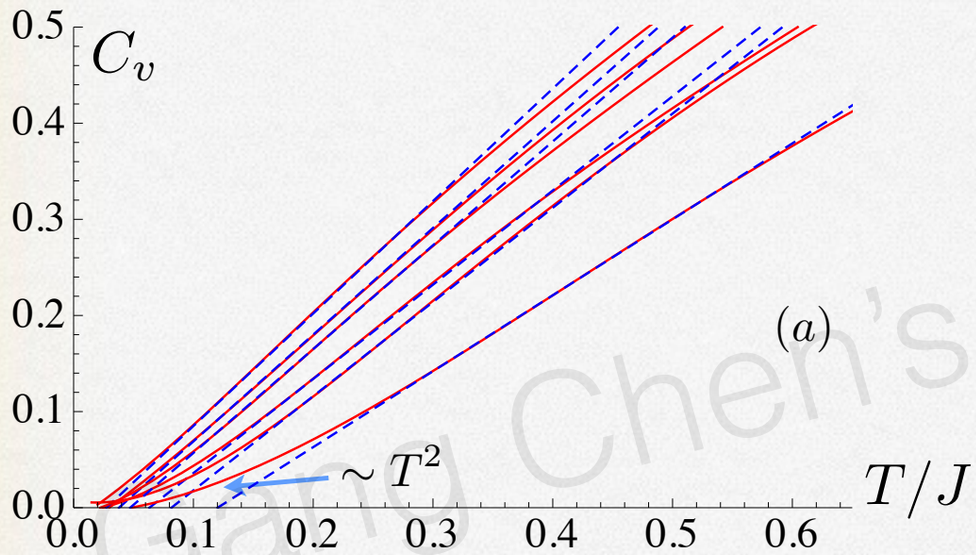

$$J_1 = J_2, 0.7J_2, 1.5J_2, 1.8J_2, 0.3J_2, 0$$

$$D \approx D_c$$

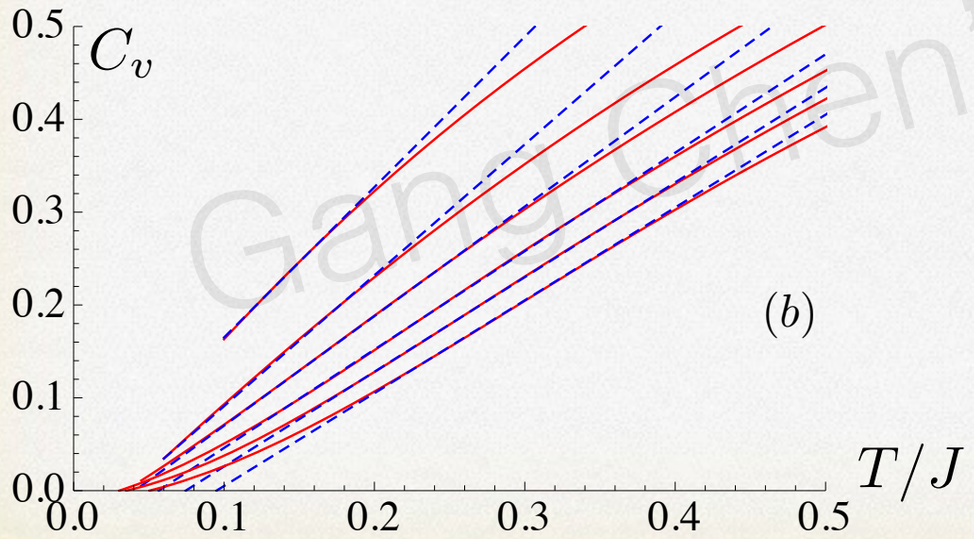

$$J_1 = 0.5J_2$$

$$D = 1.083J, 1.233J, 1.32J, 1.413J, 1.48J, 1.547J$$

$\Delta(0)/2$ D_c

Non-relativistic dispersion

$$\epsilon_{\pm,\mathbf{k}} = \sqrt{(4D + 2s_{\pm,\mathbf{k}})(\Delta(T) + s_{\pm,\mathbf{k}})}$$
$$= \sqrt{2\left[(s_{\pm,\mathbf{k}} + D + \frac{\Delta(T)}{2})^2 - (D - \frac{\Delta(T)}{2})^2\right]}$$

At QCP, relativistic dispersion

$$\epsilon_{-,\mathbf{k}} \approx \sqrt{A\Delta_1(T) + v_{\perp,k_0}^2 k_\perp^2 + v_{z,k_0}^2 k_z^2}$$

At $D = \Delta(0)/2$, non-relativistic dispersion

$$\epsilon_{-,\mathbf{k}} = \sqrt{2}(s_{-,\mathbf{k}} + D + \frac{\Delta(T)}{2})$$
$$\approx \sqrt{2}(D + \frac{\Delta_1(T) - \Delta_0}{2}) + \frac{k_\perp^2}{2m_{\perp,k_0}} + \frac{k_z^2}{2m_{z,k_0}}$$

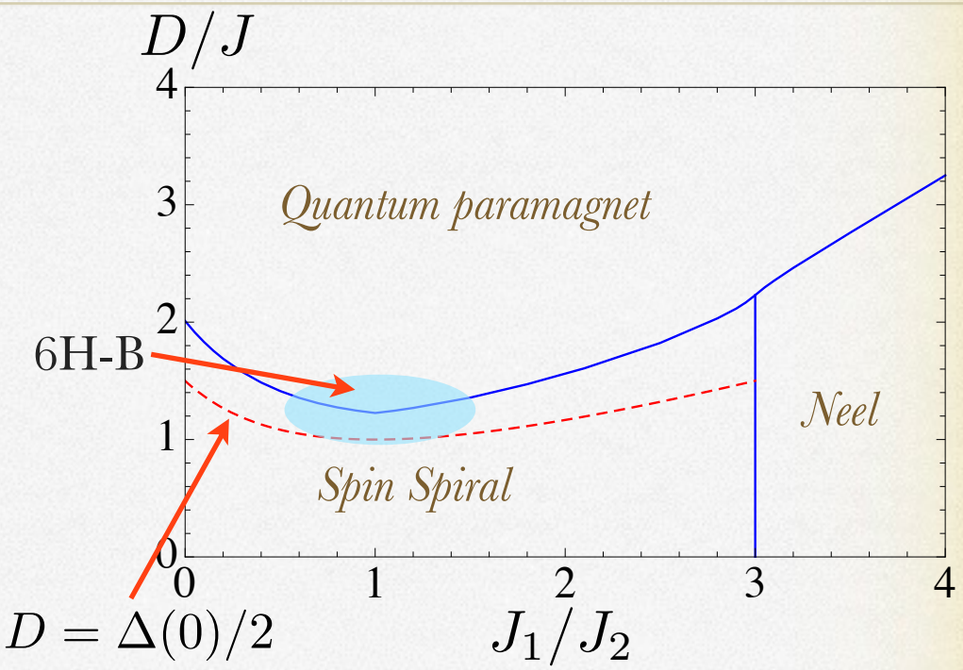

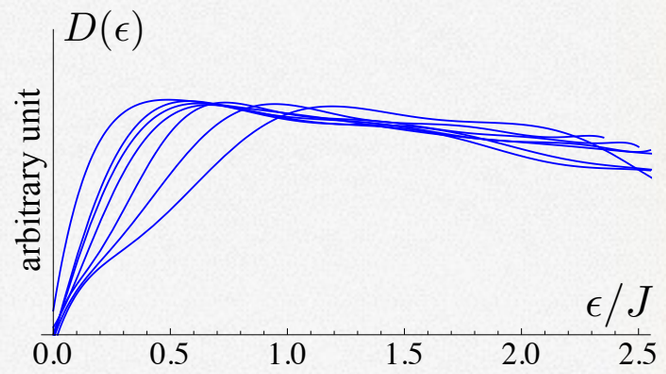

FIG. 5. (Color online) Density of states at zero temperature for different J_1/J_2 at QCP. From the leftmost curve to the rightmost curve, $J_1/J_2 = 1.0, 0.7, 1.4, 1.5, 0.5, 0.4, 0.3$ with $D = D_c$.

Comparison with Experiments

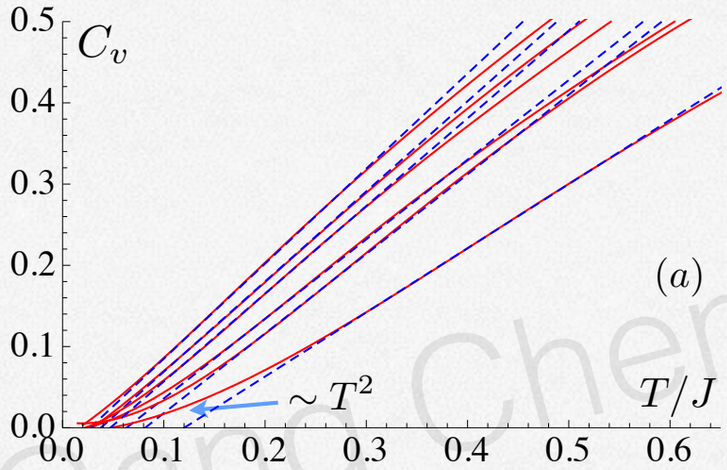

$$J_1 = J_2, 0.7J_2, 1.5J_2, 1.8J_2, 0.3J_2, 0$$

$$D \approx D_c$$

$$\chi_0^{\perp} = \frac{2\mu_0(g\mu_B)^2}{D+12J} \quad \textit{and} \quad \chi_0^{av} = 2\chi_0^{\perp}/3.$$

Experiments

$C_v(T) \simeq \gamma T^{\eta}$ with $\eta \approx 1.0(1)$

for $0.35\text{K} < T < 7\text{K}$ (or $0.02J < T < 0.34J$)

$\chi_0^{av} = 0.013\text{emu/mol}$

$\gamma = 168\text{mJ/mol-K}^2$

Wilson ratio $R = 5.6$

Prediction right at QCP with $J_1 = J_2$

$\chi_0^{av} = 0.0125\text{emu/mol}$

$\gamma = 208\text{mJ/mol-K}^2$

$R = 4.36$

SUMMARY

- We proposed and analyze a minimal J1-J2-D modal for a Ni-based triangular system
- Our prediction based on proximity to QCP is broadly consistent with experiments
- Neutron scattering and NMR may be used to confirm other predictions of the theory.

$Ba_3NiSb_2O_9$ is not exotic, but still very interesting!

Spin Liquid State in the $S = 1/2$ Triangular Lattice $Ba_3CuSb_2O_9$

H. D. Zhou,[1,*] E. S. Choi,[1] G. Li,[1] L. Balicas,[1] C. R. Wiebe,[1,2,3] Y. Qiu,[4,5] J. R. D. Copley,[4] and J. S. Gardner[4,6]

[1]*National High Magnetic Field Laboratory, Florida State University, Tallahassee, Florida 32306-4005, USA*
[2]*Department of Chemistry, University of Winnipeg, Winnipeg, MB, R3B 2E9 Canada*
[3]*Department of Chemistry, University of Manitoba, Winnipeg, MB, R3T 2N2 Canada*
[4]*NIST Center for Neutron Research, Gaithersburg, Maryland, 20899-6102, USA*
[5]*Department of Materials Science and Engineering, University of Maryland, College Park, Maryland, 20742, USA*
[6]*Indiana University, 2401 Milo B. Sampson Lane, Bloomington, Indiana 47408, USA*

(Received 12 October 2010; published 6 April 2011)

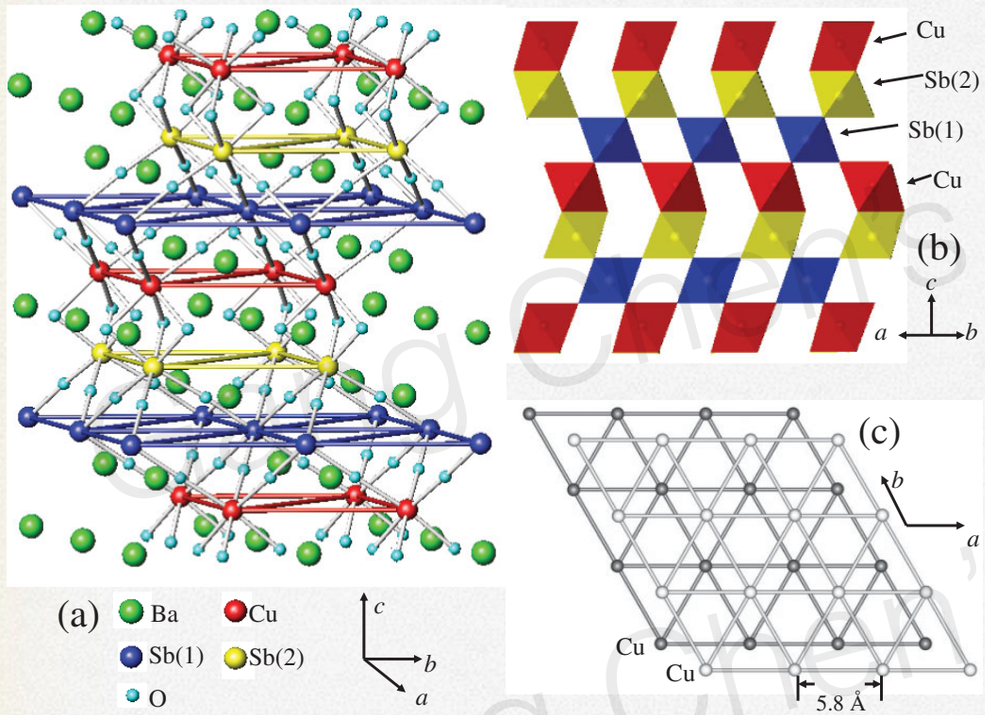

FIG. 1 (color). (a) Schematic crystal structure for $Ba_3CuSb_2O_9$; (b) The layer structure along the c axis; (c) The triangular lattice of Cu^{2+} in the ab plane.

$$g = 2.07$$

$$\theta_{\mathrm{CW}} = -55\ \mathrm{K}$$

$$z = 6,\ J/k_B = -2/3\theta_{\mathrm{CW}} = 37\ \mathrm{K},$$

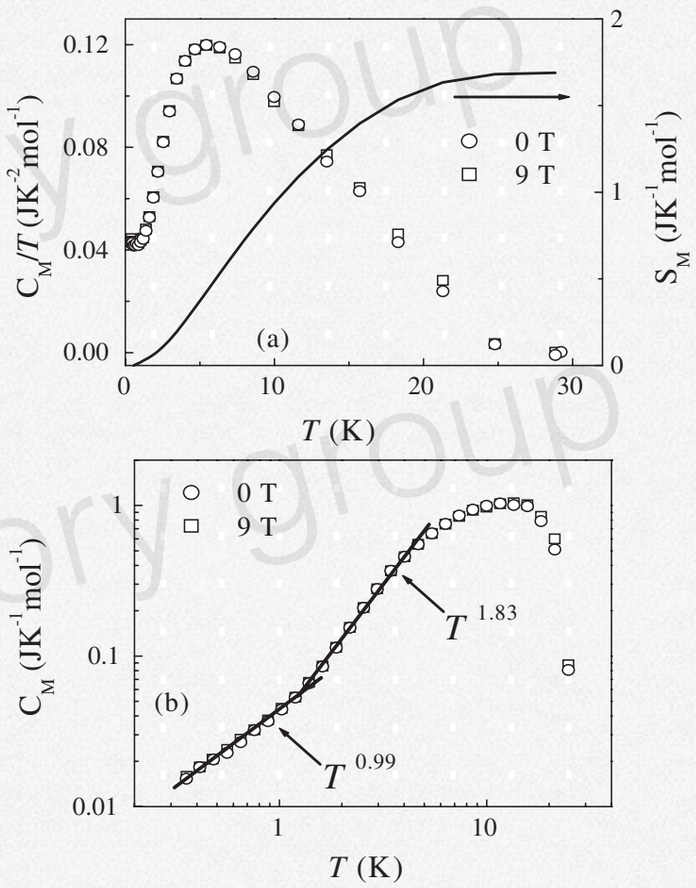

FIG. 4. (a) The temperature dependencies of C_M/T and the magnetic entropy variation S_M. (b) The temperature dependence of C_M (open symbols). The solid lines are fits as described in the text.

Spiral spin liquid?